JGR Atmospheres

RESEARCH ARTICLE
10.1029/2025JD043454

Impact of Dynamic Downscaling on the Simulation of Tropical Easterly Waves in the Intra-Americas Seas

Connor DeLaune[1,2], Vasubandhu Misra[1,2], and C. B. Jayasankar[2]

[1]Department of Earth, Ocean and Atmospheric Science, Florida State University, Tallahassee, FL, USA, [2]Center for Ocean-Atmospheric Prediction Studies, Florida State University, Tallahassee, FL, USA

Key Points:

- The dynamic downscaling generates easterly waves in the Intra-Americas Seas despite weak forcing in the driving global reanalysis
- The exit regions of some of the low-level jets generate a bias of excessive Tropical Easterly Waves in the regional model simulations
- Cumulus parameterization scheme has a significant impact in the simulation of the tropical easterly waves in the Intra-Americas Seas

Supporting Information:

Supporting Information may be found in the online version of this article.

Correspondence to:

V. Misra,
vmisra@fsu.edu

Citation:

DeLaune, C., Misra, V., & Jayasankar, C. B. (2025). Impact of dynamic downscaling on the simulation of Tropical Easterly Waves in the Intra-Americas Seas. *Journal of Geophysical Research: Atmospheres*, *130*, e2025JD043454. https://doi.org/10.1029/2025JD043454

Received 31 JAN 2025
Accepted 28 AUG 2025

Author Contributions:

Conceptualization: Connor DeLaune, Vasubandhu Misra, C. B. Jayasankar
Data curation: Connor DeLaune, C. B. Jayasankar
Formal analysis: Connor DeLaune, Vasubandhu Misra, C. B. Jayasankar
Funding acquisition: Vasubandhu Misra
Investigation: Connor DeLaune, Vasubandhu Misra, C. B. Jayasankar
Methodology: Connor DeLaune, Vasubandhu Misra, C. B. Jayasankar
Project administration: Vasubandhu Misra
Resources: Vasubandhu Misra, C. B. Jayasankar
Software: Connor DeLaune, C. B. Jayasankar
Supervision: Vasubandhu Misra
Validation: Connor DeLaune, Vasubandhu Misra, C. B. Jayasankar
Visualization: Connor DeLaune, C. B. Jayasankar

Abstract We analyze two 16-year dynamically downscaled simulations for their Tropical Easterly Waves (TEWs) from global reanalysis of the atmosphere and ocean over the Intra-Americas Seas (IAS) region, centered over Central America. We implemented two versions of a coupled ocean-atmosphere Regional Climate Model (RCM), each run at 15 km grid resolution and differing solely in their cumulus parameterization schemes. Our analysis reveals that the RCMs were able to generate TEWs in the domain even though the global atmospheric reanalysis forcing the regional models generated a few TEWs. This seems to suggest an in situ generation of these TEWs in the domain, which is consistent with earlier studies that examined TEW over the IAS region. There were also crucial differences between the two versions of the RCMs, suggesting that the cumulus parameterization scheme has an important bearing on the generation of TEWs in the simulation over this region. In one instance of the RCM simulation, the response of the TEW was much stronger, where the convective activity was enhanced with both convective and stratiform precipitation associated with TEW higher than the other cumulus scheme used in the other RCM simulation. However, the limitations and advantages of the impacts of the two cumulus parameterization schemes on the overall simulation of TEWs refrain us from claiming one scheme is superior to the other. Nonetheless, the study highlights the importance of the cumulus scheme and the benefit of dynamic downscaling on the simulation of TEWs.

Plain Language Summary Tropical Easterly Waves (TEWs) is an important feature of the Intra-Americas Seas (IAS) region, which spawns many of the Tropical Cyclones (TCs) in the region. This study analyzes two Regional Climate Model (RCM) simulations at 15 km grid resolution forced by a much coarser global reanalysis of the atmosphere (2.5° grid) and ocean (0.5° grid) centered over Central America. Our analysis indicates that the regional models successfully produced TEWs within the domain, despite minimal TEWs resolved in the global atmospheric reanalysis data used to force them. This suggests that the TEWs were generated locally within the domain, aligning with previous studies on TEWs in the IAS region. The results also highlight the benefit of downscaling using a regional model. The study also focuses on the importance of the cumulus parameterization scheme in the simulation of the TEWs in the regional models. Although we could not conclude that one cumulus scheme was superior to the other, we reveal the features of the TEW that were modulated in the two simulations of the regional model such as their amplitude and wavelength, frequency of the TEWs growing to TCs, besides the differences in the mean wind circulation and precipitation associated with the TEWs.

1. Introduction

Tropical Easterly Waves (TEWs) are westward propagating waves, which are ubiquitous in the tropics and occur throughout the year. A large fraction of these TEWs originating from northern Africa (also referred to as African Easterly Waves [AEWs]), result in tropical cyclogenesis especially in the tropical Atlantic and east Pacific basins with nearly 85% of the Atlantic major hurricanes originating from these waves (Agudelo et al., 2011; Landsea, 1993). Similarly, the tropical eastern Pacific basin designated as the most active tropical cyclogenesis region (in terms of genesis events per unit area per unit time; Gray, 1968; Molinari et al., 2000) has most of its Tropical Cyclone (TC) events triggered by a TEW (Avila & Pasch, 1992). Therefore, these TEWs or AEWs are of immense importance to understand their genesis, evolution, and variations. It may however be noted that only 14%–18% of the TEWs develop into TCs in the Atlantic basin (Agudelo et al., 2011; Avila et al., 2000; Pasch & Avila, 1994). It is slightly higher in the eastern Pacific with about 25% of TEWs developing into TCs (Molinari et al., 1997). The AEWs typically have a phase speed of 5–10 ms^{-1} and a period of 3–5 days with a wavelength of ~2,000 km (Avila & Pasch, 1992). There are many theories to explain their existence including the combined

Writing – original draft: Vasubandhu Misra
Writing – review & editing: Connor DeLaune, Vasubandhu Misra, C. B. Jayasankar

barotropic-baroclinic instability of the African easterly jet (Burpee, 1972, 1974; Diaz & Aiyyer, 2015), interaction of AEW with diabatic heating from convective instability leading to its growth (Mekonnen et al., 2006; Thorncroft et al., 2008), mountain lee waves evolving to AEW (Lin et al., 2005), inertial instability from cross-equatorial pressure gradients (Toma & Webster, 2010), and from breakdown of the ITCZ (Ferreira & Schubert, 1997).

Regional atmospheric models have been used earlier to understand the TEWs (e.g., Dominguez et al., 2020; Hsieh & Cook, 2007; Lin et al., 2005; Rydbeck et al., 2017; Seo et al., 2008). These studies generally have been run at a coarser resolution relative to this study and for shorter periods ranging from a case study of a developing Tropical Cyclone (TC; e.g., Lin et al., 2005) to several (∼5–10) years of seasonal simulations (e.g., Rydbeck et al., 2017). Many of these studies have provided insight into TEWs. For instance, Rydbeck et al. (2017) showed in their regional modeling study that a large fraction of easterly waves in the tropical east Pacific basin is generated locally from the westward migration of diurnal convection from the Panama Bight (Gulf of Panama) region to the east Pacific warm pool region where it matures to a meso-scale convective system and spawns TEWs. Furthermore, by reducing the terrain height in the region, they were able to significantly reduce the local generation of easterly waves in the east Pacific but not completely eliminate it to suggest that some of the TEWs in the east Pacific are AEWs (Rydbeck et al., 2017). Similarly, Seo et al. (2008) highlighted the importance of grid resolution of atmospheric models to simulate AEWs. They conducted a comparison between two coupled ocean-atmosphere regional models, which differed solely in their atmospheric model grid resolution. The results indicated that a more realistic precipitation climatology and seasonality over the northern tropical Atlantic Ocean was achieved through improved AEW-related moisture convergence and convection processes in the finer resolution atmospheric model as opposed to a coarser atmospheric model coupled to a relatively fine resolution ocean model. In another regional modeling related study, Dominguez et al. (2020) indicated that the TEWs contribute significantly to the seasonal rainfall over northern South America and Central America and highlighted the importance of model physics in the simulation of TEWs.

In a related study, Fuentes-Franco et al. (2015) showed that model physics and resolutions had differing impacts on the seasonal simulations of TCs in the tropical east Pacific and Atlantic Oceans. For example, they found that model resolution had more of an influence in the east Pacific with coastal topography playing a critical role in simulating TC genesis in the east Pacific. Furthermore, they find that mass flux convection schemes perform better in simulating seasonal features of TCs in the Atlantic. Diro et al. (2014) also found similar sensitivity of TC genesis to cumulus schemes in their regional modeling study.

In this study, we are examining the impact of dynamic downscaling a relatively coarse atmospheric reanalysis (NCEP R2 available at 2.5°; Kanamitsu et al., 2002) with a comparatively high resolution (15 km grid) coupled ocean-atmosphere regional model centered over Central America on the simulation of the TEWs. Additionally, we are also examining the impact of cumulus parameterization in the regional model by examining two separate 16-year simulations with two different cumulus parameterization schemes.

The regional domain covers portions of the Intra-Americas Seas (IAS) that include the western hemisphere warm pool (Wang & Enfield, 2001; cf. Figure 1 in Amador, 2008). The region is characterized by mid-level jets at 600 hPa, one around 15°N over the southwestern Caribbean Sea and another around 2°N with peak magnitudes around 6–7 ms^{-1} (cf. Figure 1 in Torres et al., 2021). The region also features the Caribbean Low-Level Jet (CLLJ) with its biannual seasonal cycle and resides around 13°N between 73°W and 95°W at 925 hPa with peak winds ∼12 ms^{-1} (Amador, 1998; Cook & Vizy, 2010). Several studies have suggested that the CLLJ can enable growth of TEWs from barotropic instability (Molinari et al., 2000; Serra et al., 2010). Recently, Torres et al. (2021) showed that easterly waves in the tropical eastern Pacific can be triggered by finite-amplitude transient heating in the vicinity of the mid-level jet at about 15°N over the IAS region. Furthermore, they show sensitivity of the easterly waves to latent heat profiles at this location (in the vicinity of the mid-level jet) with the stratiform type of convection showing the strongest response while the shallow convection profile had the weakest response. The deep convective heating profile forced a response that was weaker than the stratiform but stronger than the shallow convective heating profile.

In the following section, we describe the regional model used for the study and the design of the model experiments. This is followed by a discussion of the methodology to diagnose the TEWs and the composites constructed for the analysis. In Section 4, we describe the results followed by conclusions in Section 5.

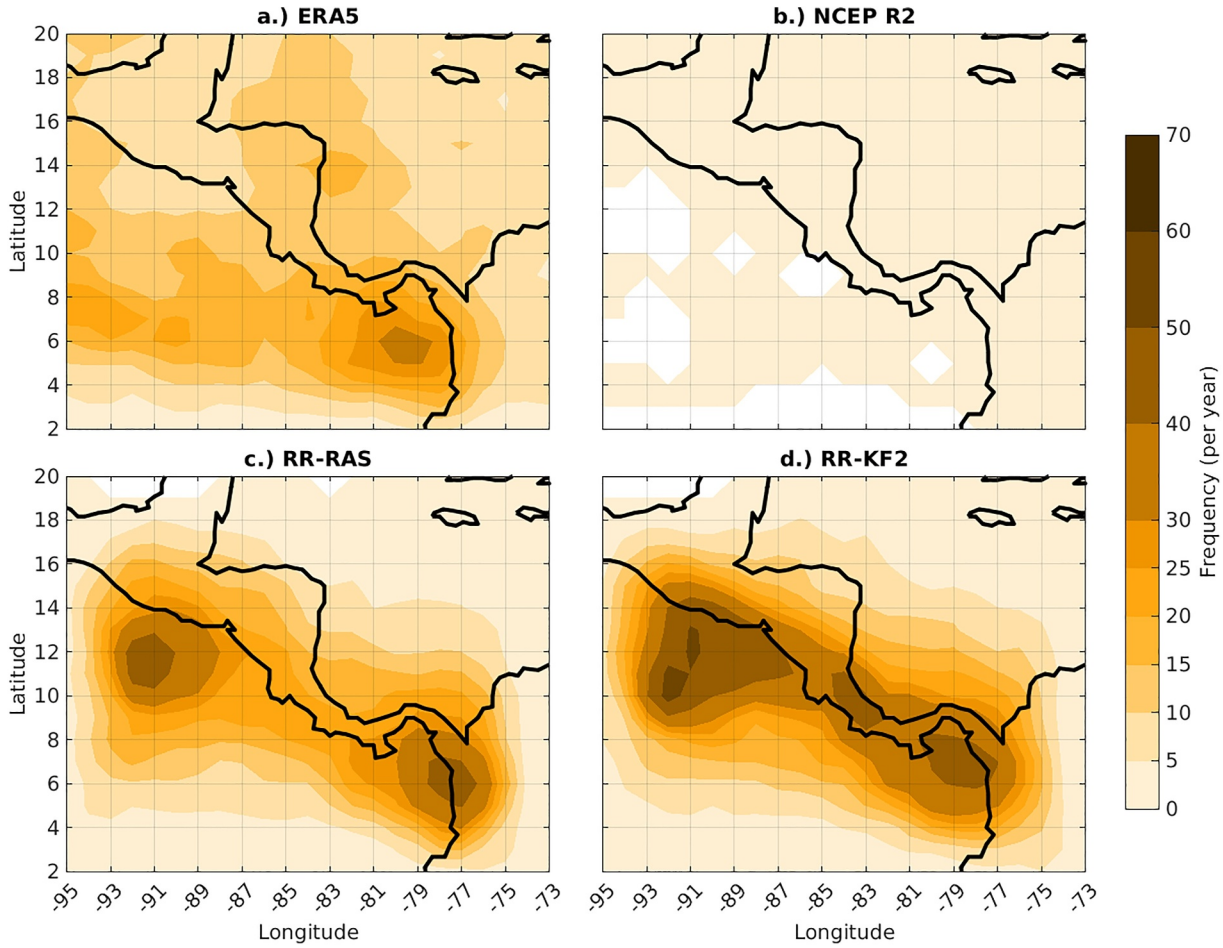

Figure 1. May–November average tropical easterly wave track density at 600 hPa for (a) ERA5, (b) NCEP R2, (c) RR-RAS, and (d) RR-KF2 for 1986–2001.

2. Model Description and Experiments

The model utilized in this study is the Regional Spectral Model-Regional Ocean Modeling System (RSM-ROMS), which has been widely used for regional climate downscaling over many regions around the globe (Ham et al., 2016; Li et al., 2012; Misra et al., 2022). In this study, RSM-ROMS is configured with a 15 km grid spacing for both the atmospheric and oceanic components of the model. Both these components share identical grid discretization, which means the atmospheric fluxes from the atmosphere to the ocean and SST from the ocean to the atmosphere are exchanged at 1-hr intervals directly without using any flux coupler or interpolations.

The RSM follows originally from Juang and Kanamitsu (1994), which has gradually undergone development over the years with the latest version used for this study detailed in Misra et al. (2022). There are 28 terrain following $\sigma\left(=\frac{p}{p_s}\right)$ levels reaching up to ~2 hPa in RSM and the physics of the model including a non-local boundary layer scheme (Hong & Pan, 1996), the four-layer community Noah land surface model (Ek et al., 2003), long wave radiation (Chou & Lee, 1996), shortwave radiation (Chou & Suarez, 1994), shallow convection (Tiedtke, 1983), prognostic clouds (Zhao & Carr, 1997), gravity wave drag (Alpert et al., 1988), and deep convection schemes of Relaxed Arakawa Schubert (RAS; Moorthi & Suarez, 1992) and Kain-Fritsch version 2 (KF2; Kain & Fritsch, 1993).

The ROMS is a free-surface, terrain following a primitive equation model with 30 vertical stretched terrain (S) levels with higher resolution provided in the upper ~500 m of the ocean (Haidvogel et al., 2000; Shchepetkin & McWilliams, 2005). It uses the Arakawa-C grid for horizontal discretization. ROMS include a local closure scheme of 2.5 level turbulent kinetic energy (Mellor & Yamada, 1982), generic length scale parameterization

Table 1
A Brief Outline of the Verification of Data Used in the Study

Variable	Data set	Grid spacing	Period of verification	Temporal resolution	Reference
Precipitation	Integrated Multi-satellitE Retrievals for GMP version 7 (IMERG)	0.1° × 0.1°	2001–2022	6 hourly	Huffman et al. (2019)
SST	Optimally interpolated SST version 2 (OISST)	0.25° × 0.25°	1986–2001	Daily	Reynolds et al. (2007)
Upper air variables	European ReAnalysis (ERA5)	0.25° × 0.25°	1986–2022	6 hourly	Hersbach et al. (2020)
Tropical cyclone fixes	Hurricane Data version 2 (HURDAT2)		1986–2000	6 hourly	Landsea and Franklin (2013)

(Umlauf & Burchard, 2003), second order biharmonic diffusion (Ezer et al., 2002), and boundary layer formulation following Large et al. (1994).

For this study, we integrate two versions of RSM-ROMS separately for a period of 16 years (1986–2001). In one version of RSM-ROMS, we use the RAS convection scheme, and we will refer to this model run as RR-RAS and in the other we use the KF2 convection scheme, hereafter referred to as RR-KF2. Both the model integrations were forced at the lateral boundaries of the atmosphere and ocean by NCEP R2 reanalysis and Simple Ocean Data Assimilation v 2.2.4 (SODA; Carton & Giese, 2008), respectively. Both the model integrations were initialized with R2 for the atmosphere and SODA for the ocean. Given earlier discussion of the importance of diabatic heating in the simulations of TEWs, we selected two deep convection schemes that are extensively used in climate modeling studies (e.g., Ham & Hong, 2013; He et al., 2015; Peishu et al., 2017). These schemes differ in concept with RAS based on quasi-equilibrium theory of convection acting to maintain equilibrium with the generation of available energy from large-scale processes while KF2 triggers convection when a certain criterion of instability and moisture availability is met. The implementation of the scheme is also quite different, with clouds in RAS represented by a spectrum of cloud types with detrainment level at different pressure levels while a single column convective cloud model is used in the KF2 scheme.

The model simulations are verified with the data outlined in Table 1 below and where applicable, the model data were interpolated to observational grid when differences with observations were computed.

3. Methodology for Diagnostics

The TEWs were identified at 850, 700, and 600 hPa using an objective tracking algorithm from Belanger et al. (2017) applied to ERA5, RR-RAS, RR-KF2, and NCEP R2. The algorithm uses the advection of curvature vorticity on a 2-D wind field to track TEWs along with additional criteria: (a) zonal wind being less than 2.5 ms^{-1}, (b) curvature vorticity anomaly exceeding the 66th percentile of all the anomalies, (c) advection of curvature vorticity anomaly equaling to 0 s^{-2}, (d) TEW lasting at least 2 days, and (e) median speed being between −25 m/s and −2 m/s to ensure eastward propagation. TEWs were identified from 1986 to 2022 in ERA5 and only for 1986–2001 in RR-RAS, RR-KF2, and NCEP R2.

Track densities for each data set and pressure level were analyzed using the centroid point of each TEW axis at a 2° resolution. Wavelengths were calculated using a function from Belanger et al. (2017) which used a factor four scale to measure the TEW zonal extent based on the direction of the TEW propagation, and amplitudes were computed using the distance between the wave centroid location and the northern most point. To analyze TEW vorticity, a 5° box was utilized around the wave centroid point to calculate the areal vorticity before being averaged across the entire TEW lifespan. A 5° box was selected to ensure that just the wave trough was being incorporated into the calculations. To make this study more robust, only the TEWs that exceeded an average areal vorticity of 0 s^{-1} (positive vorticity) were analyzed. For the precipitation analysis, a 10° box was used since there is uncertainty in the extent of TEW influence on the environment. Similar TEW precipitation studies vary between what distance to attribute precipitation around a TEW axis with Dominguez et al. (2020) utilizing a 15° box and Hollis et al. (2024) using a 500 km radius around the wave center, so a consensus was applied in this study.

The tracks of the Tropical Storms (TS; >17 m/s) were identified for RR-RAS and RR-KF2 using the TempestExtremes algorithm, an automated Lagrangian pointwise feature tracker following (Ullrich &

Zarzycki, 2017). This algorithm consists of two steps: (a) finding suitable candidates at each time step using threshold-based criteria that isolate points within the closed contours and (b) tracking these candidates over time by linking neighboring ones and eliminating those that do not move consistently. This study identifies the systems based on the mean sea level pressure (MSLP) and upper-level geopotential layer thickness criteria from the 6-hourly interval data sets following Ullrich et al. (2021). First, candidate tropical systems (TS) are identified by evaluating the MSLP: it must increase by at least 200 Pa over a 5.5° great-circle distance from the candidate point. Second, the upper-level warm core is assessed by examining the geopotential layer thickness between 300 hPa and 500 hPa, which must decrease by at least 3 m (modified from the original threshold of 6 m) over a 6.5° great-circle distance. To ensure system intensity, the 10-m wind speed must exceed 10 m/s for at least four 6-hr time steps. Additionally, the system must maintain a surface geopotential below 150 m for no fewer than 24 hr (i.e., four 6-hourly steps).

4. Results

4.1. Climatological Frequency of Tropical Easterly Waves

We show in Figure 1 the climatological frequency of TEWs at 600 hPa for May through November (North Atlantic and East Pacific TC season). ERA5 reanalysis, which is used as a validation data set in Figure 1a shows the highest frequency of TEWs (>30 per year) just south of Gulf of Panama and a broader region of more moderate activity (∼10–20 per year) zonally in eastern Pacific and along the Caribbean Sea coast of the isthmus. The NCEP R2 reanalysis in Figure 1b on the other hand shows marginal TEWs with a frequency of less than <2 per year across the domain. The downscaling in RR-RAS substantially increases the TEWs relative to NCEP R2 (Figure 1c), especially along the Pacific slope of Central America with the frequency raised to at least 40 per year along the coast of Colombia and off the coast of El Salvador while along the Caribbean coast it is ≤20 per year. It may be noted that NCEP R2 displayed the lack of barotropic instability (determined by the lack of reversal of signage of the meridional gradient of potential vorticity) in the east Pacific (not shown). In contrast, RR-KF2 raises the count of TEWs to well over 40 per year along the Pacific coast of Central America while along the Caribbean coast it is ≥20 per year. Incidentally, the bias of excessive TEWs off the Pacific coasts of Panama and Nicaragua in both the model simulations are close to the exit region of the Panama and Papagayo Low-Level Jets (LLJs). Furthermore, both versions of the regional model simulations differ in their spatial distribution of TEWs from ERA5 substantially. For instance, the zonal distribution of high frequency of TEWs in the Pacific in ERA5 is not replicated in either of the two model simulations. However, considering the boundary forcing for both simulations being NCEP R2 which shows very few TEWs, it is interesting to note that the model simulations can generate significantly higher number of TEWs. It may be noted that some of the differences between the regional model simulations could be partly explained by the corresponding bias in the SST shown in Figure S1 in Supporting Information S1. We observe in Figure S1 in Supporting Information S1 that RR-RAS has a cold SST bias along the coastal oceans which is comparatively reduced in RR-KF2. Therefore, the relatively severe cold bias along the Pacific coast of Central America in RR-RAS reduces convective activity (or precipitation) in the region (Figure S2 in Supporting Information S1), thereby reducing the likelihood of the growth of TEW. In a related study, Druyan and Fulakeza (2011) show similar sensitivity of TEW simulations to SST. It should be mentioned that the Caribbean Low Level Jet (CLLJ) in both the regional model simulations are found to be nearly identical (Figure S3 in Supporting Information S1). This is important to note because CLLJ is known to play a critical role in modulating TC genesis over the Caribbean Sea region from its control over vertical shear in the Caribbean Sea (Amador, 2008; Wang, 2007). There are many other LLJs in the region that result from the gaps in the mountain ranges of Central America that could serve as a source of TEWs and tropical cyclogenesis (Holbach & Bourassa, 2014; Molinari et al., 1997; Molinari & Vollaro, 2000; Zehnder, 1991). Similar to the CLLJ, the Papagayo, Panama, and Tehuantepec LLJs are quite similar in RR-RAS and RR-KF2 simulations (Figure S3 in Supporting Information S1).

Similarly, Figure 2a shows the climatological frequency of TEWs at 700 hPa with TEW showing maximum frequency over northeastern Pacific along 6°N latitude in ERA5. These TEWs in ERA5, which is so close to the equator appears to be associated with the secondary mid-level jet around 2°N mentioned in Torres et al. (2021). However, NCEP R2, like at 600 hPa (Figure 1b), shows insignificant TEWs (Figure 2b). RR-RAS, however, enhances the TEW activity from NCEP R2, especially along the Pacific Coast of Central America (Figure 2c) and is further enhanced in RR-KF2 (Figure 2d). The spatial pattern of the frequency of TEWs in both the regional

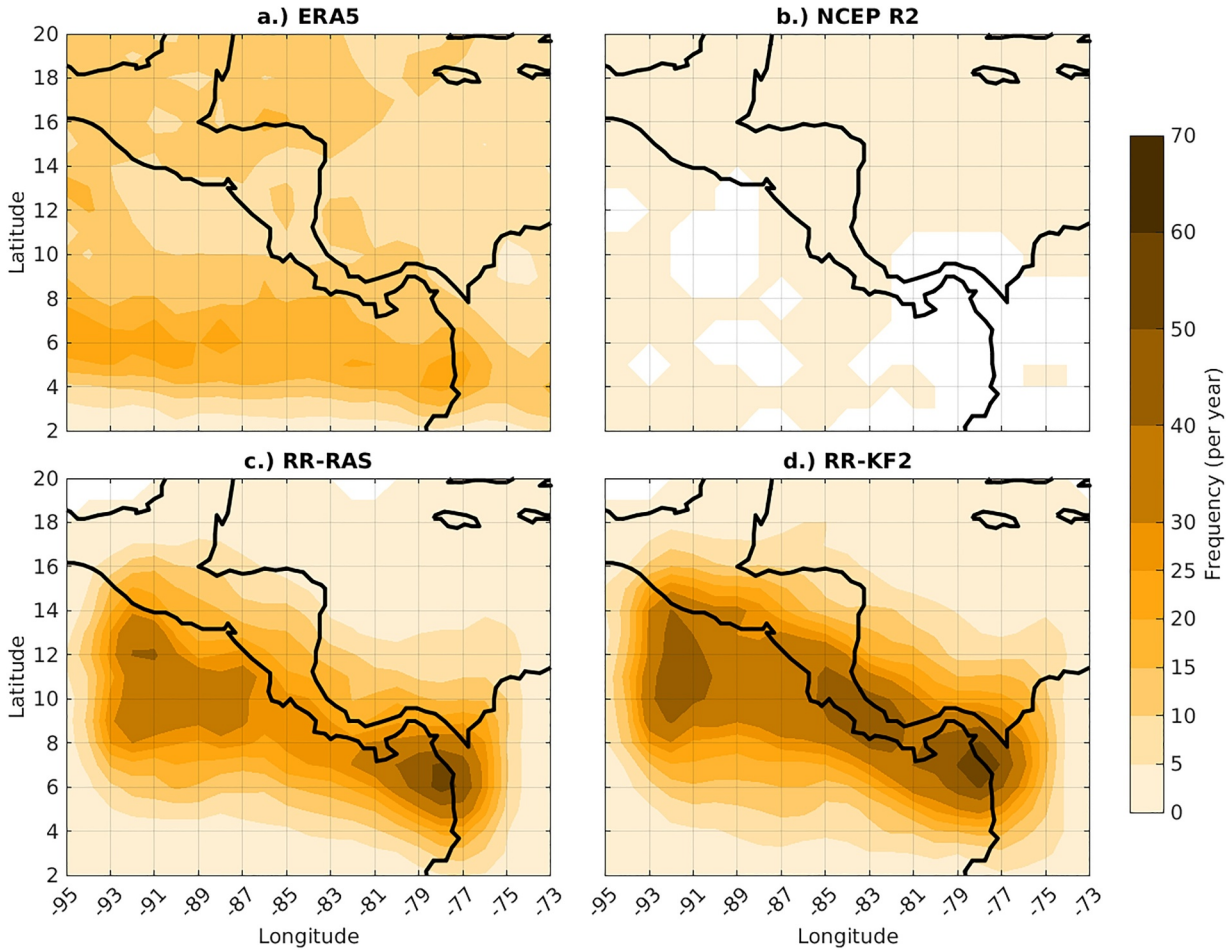

Figure 2. May–November average tropical easterly wave track density at 700 hPa for (a) ERA5, (b) NCEP R2, (c) RR-RAS, and (d) RR-KF2 for 1986–2001.

model integrations are aligned with the Central American isthmus, with RR-KF2 showing greater number of TEWs over the isthmus and along the Pacific Coast of Nicaragua and El Salvador.

At 850 hPa, the Pacific Coast of Panama and Colombia show a high number of TEWs around 6°N and further west over the open oceans in ERA5 (Figure S4a in Supporting Information S1). On the other hand, NCEP R2 continues to show an insignificant number of TEWs (Figure S4b in Supporting Information S1). However, both RR-RAS (Figure S4c in Supporting Information S1) and RR-KF2 (Figure S4d in Supporting Information S1) show a much higher number of TEWs than NCEP R2, with the model simulations showing far more TEWs along both the coasts and over the isthmus. Overall, from these figures (Figures 1 and 2, and Figure S4 in Supporting Information S1) it is notable that the regional models can develop TEWs in the domain when the large-scale forcing from NCEP R2 had barely any such activity, suggesting the potential for local generation of these waves and the benefit of dynamic downscaling. Furthermore, the regional models generate far more TEWs compared with ERA5 at all three pressure levels (600, 700, and 850 hPa).

4.2. Wavelength of the Tropical Easterly Waves

The probability distribution of wavelength of the TEWs at 600, 700, and 850 hPa are shown in Figure 3. It is notable that both in ERA5 and NCEP R2 TEWs with wavelengths of ∼2,000 km having the most probability at all three pressure levels. However, NCEP R2 shows a wider distribution of wavelengths of TEWs compared with ERA5 at all pressure levels. In comparison, RR-RAS and RR-KF2 show a shorter wavelength of TEWs of ∼1,300 and ∼1,400 km with the highest likelihood, respectively. The probability distribution of the wavelengths of TEWs in both these models is much narrower with the longer wavelengths (>2,000 km) underestimated compared with

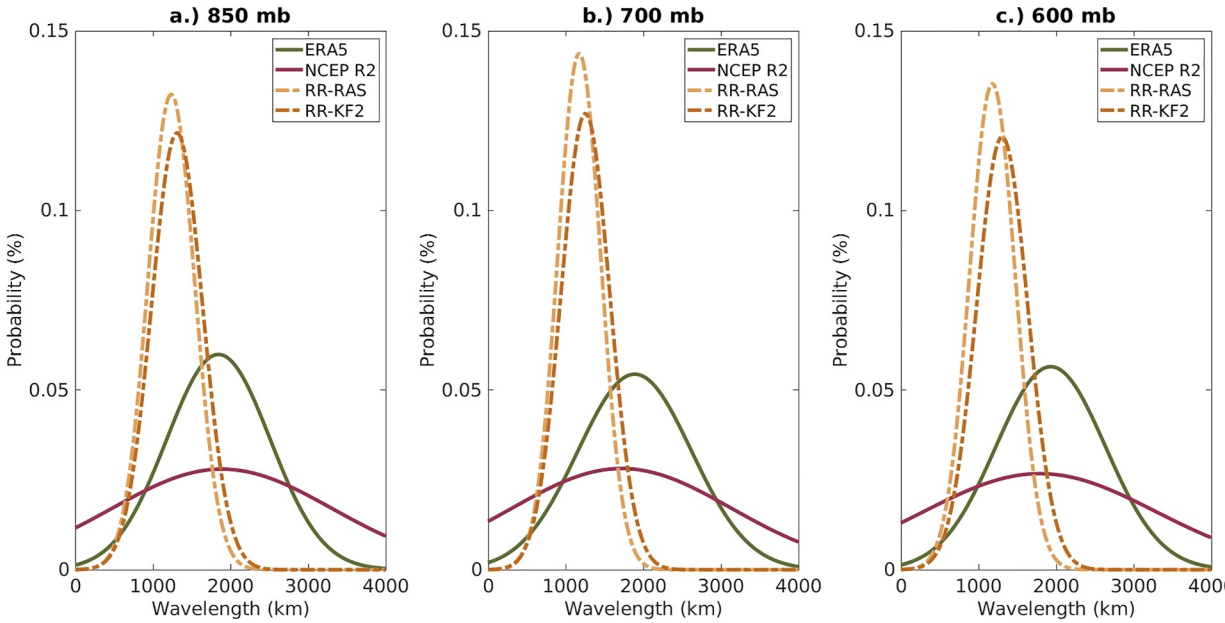

Figure 3. Probability density function of May–November average tropical easterly wave wavelengths at (a) 850 hPa, (b) 700 hPa, and (c) 600 hPa for 1986–2001. The ordinate represents the probability of the waves of a specific wavelength across the spectrum of wavelengths of the Tropical Easterly Waves in the data set.

ERA5. At 700 hPa (Figure 3b), the distribution of TEW becomes slightly sharper than in the other two pressure levels in both RR-RAS and RR-KF2 simulations (Figures 3a and 3c). Overall, Figure 3 suggests that the regional models tend to produce TEWs with shorter wavelengths more regularly than the global reanalysis of ERA5 and NCEP R2, which displays a broader distribution of wavelengths. It is possible that the bias of shorter wavelengths in the regional model simulations could have stemmed from the limited domain of the regional models. Future studies could potentially investigate the size of the regional domain on the wavelength of the simulated TEWs in the regional model simulations.

4.3. Amplitude of Tropical Easterly Waves

The probability distribution of the amplitudes of the TEWs are shown in Figures 4a–4c for the three pressure levels. The regional models display slightly lower amplitude TEWs with a higher probability than ERA5 at all three pressure levels. ERA5 shows the widest distribution of amplitudes of TEWs at all three pressure levels. The NCEP R2 reanalysis shows a narrower distribution than ERA5 with the most probable amplitudes being weaker than ERA5. The most probable amplitudes in the regional models are comparable to each other and NCEP R2 at 700 hPa. Furthermore, the distribution of the amplitudes of TEWs in the regional models are slightly narrower than either of the two reanalyzes, indicating that the models tend to underestimate the frequency of higher and lower amplitude TEWs compared with ERA5 and NCEP R2.

4.4. Lower Tropospheric Circulation

Figure 5 displays the composite climatological wind difference at 925 hPa when TEWs are present compared with when they are not present at 600 hPa within the model domain. It is apparent from this figure that the Central American monsoon gyre is modulated when TEWs are present at 600 hPa in all four panels of Figure 5. However, the magnitude of the wind anomalies and the center of the anomalous gyre circulation differ across the data sets (Figure 5). For instance, in ERA5, the center of the anomalous gyre is located around 14°N and 85°W (Figure 5a). In NCEP R2, the anomalies are far larger in magnitude and the center of the anomalous gyre is around 17°N and 90°W (Figure 5b). The larger anomalies displayed by NCEP R2 in Figure 5b is also a result of the composite developed from a much smaller sampling of TEWs in the data set. Furthermore, in NCEP R2, the southern flank of the gyre shows more extensive and stronger wind anomalies while in ERA5 it is the eastern flank that shows stronger anomalies. Similarly, RR-RAS and RR-KF2 also show the anomalous monsoon gyre with the center displaced to around 16°N, 85°W and 18°N, 83°W, respectively. Additionally, the wind anomalies are stronger

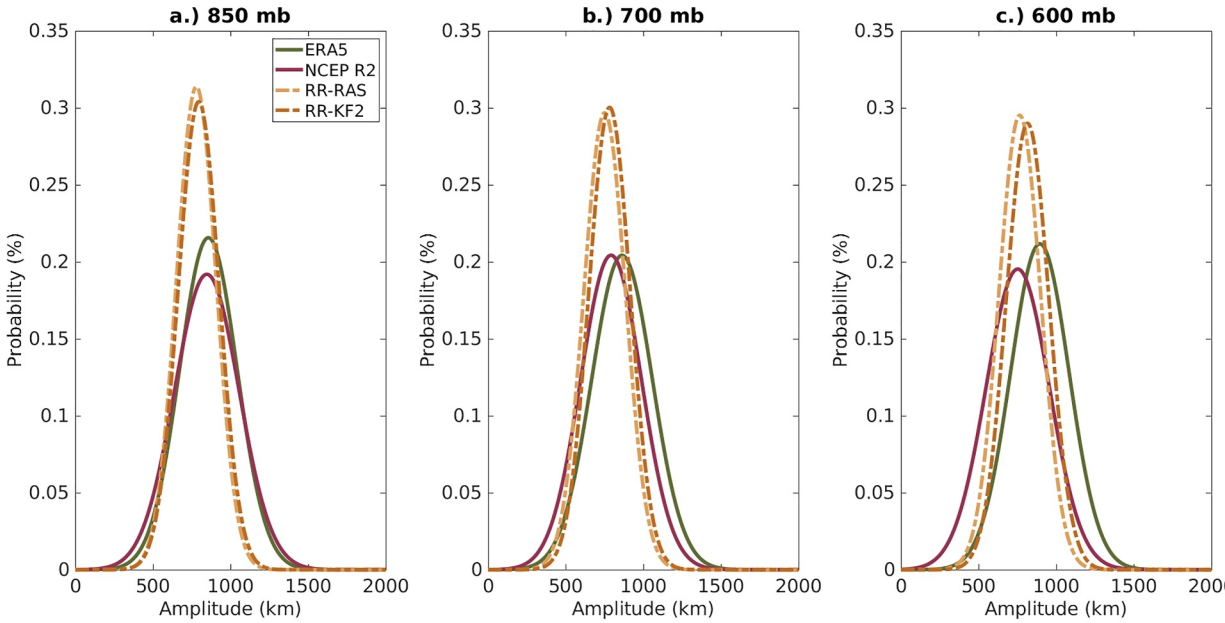

Figure 4. Probability density function of May–November average tropical easterly wave amplitudes at (a) 850 hPa, (b) 700 hPa, and (c) 600 hPa for 1986–2001. The ordinate represents the probability of the waves of specific amplitude across the spectrum of amplitudes of the Tropical Easterly Waves in the data set.

and extensive on the southern flank of the gyre in RR-RAS while in RR-KF2 the wind anomalies are comparatively weaker and stronger in the southeastern flank of the anomalous gyre. In summary, composite 925 hPa wind anomalies in Figure 5 suggest that the monsoon gyre is weakly strengthened in both model simulations and ERA5 by the TEWs. This is not surprising given that the TEWs are further equatorward to the Central American monsoon gyre. Figure 5 shows that the presence of the TEWs essentially weakens the prevailing easterly flow over the IAS. Qualitatively, similar figures are obtained for wind composite differences at 925 hPa based on TEWs at the two other pressure levels (not shown). It may be noted that several studies have suggested that interactions of the TEWs with monsoon troughs can lead to cyclogenesis (McBride & Zehr, 1981; Molinari et al., 2000).

4.5. Low-Level Vorticity

In Figure 6, we show the distribution of the vorticity in the trough axis of the TEW detected at 600, 700, and 850 hPa. In ERA5, the distribution of vorticity is wide and skewed to the right indicating higher probability toward larger vorticity. NCEP R2 shows a comparable distribution, although the distribution is narrower than ERA5. Both the model integrations display a relatively much narrower distribution with a far less positive skewness but more kurtosis than ERA5 or NCEP R2. Furthermore, between the models, RR-RAS shows a marginally smaller spread of vorticity than RR-KF2 at all pressure levels but with slightly higher kurtosis. These distributions of higher likelihood of weaker vorticity in the regional models are consistent with the weaker amplitude of the TEWs compared with ERA5 shown earlier and weaker precipitation response discussed in the following sub-section.

4.6. Precipitation

The differences in the precipitation composites in Figure 7 are revealing. Figure 7 shows the percentage of total precipitation (P) from TEWs at 600 hPa (computed by summing all precipitation observed within a 10° box around the wave centroid point and dividing by the total precipitation across May–November) from ERA5, RR-RAS, and RR-KF2, respectively. In Figure 7a, ERA5 shows the largest contribution of precipitation from TEWs over the Caribbean Sea while in both the regional model simulations the largest contribution is centered around the isthmus and is in the southern part of the domain (Figures 7a and 7b). The relatively large proportion of rainfall in northern Caribbean Sea in ERA5 (Figure 7a) is co-incident with corresponding high density of TEWs (Figure 1a). Likewise, the distribution of rainfall in Figures 7b and 7c is associated with the TEW track densities

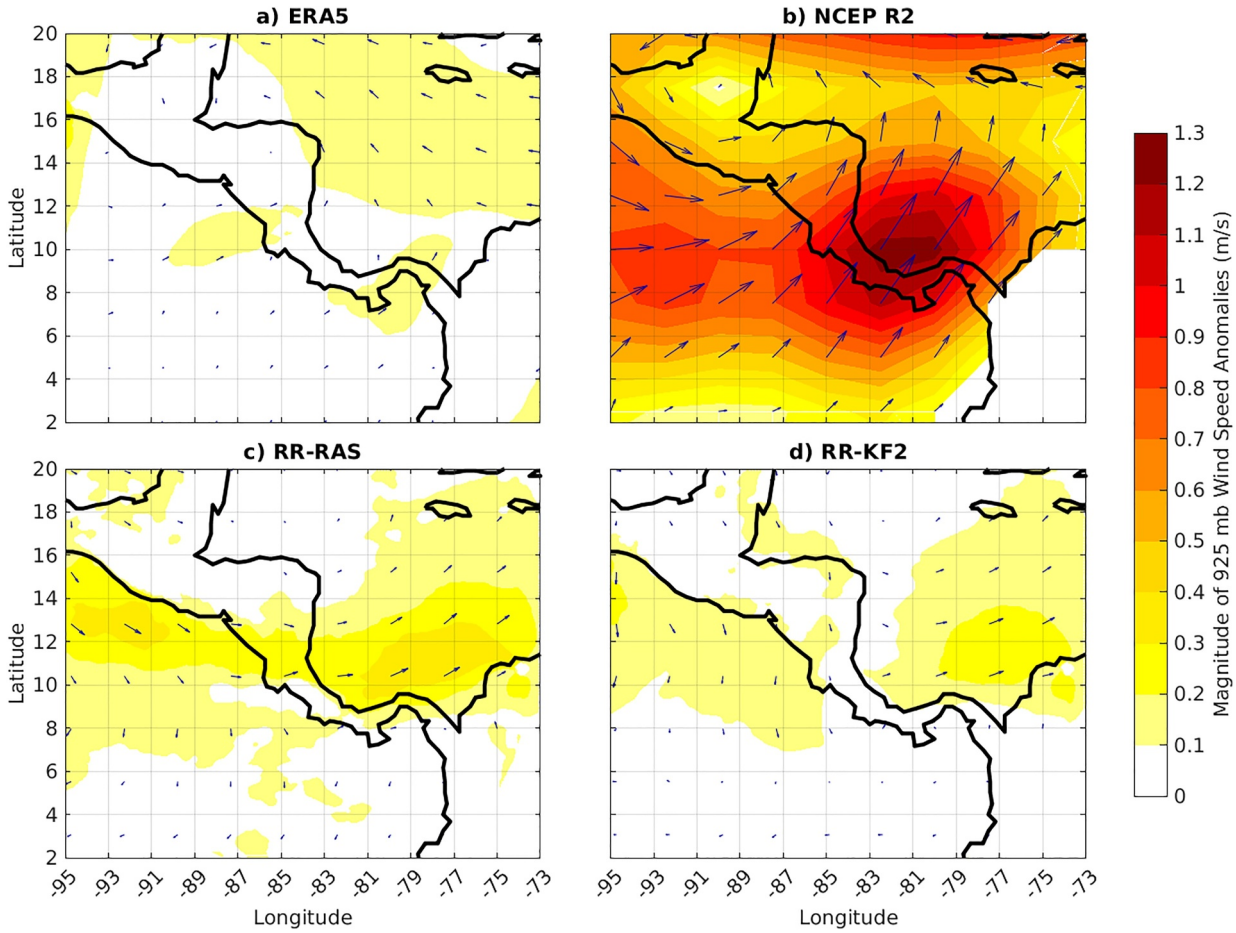

Figure 5. The composite 925 hPa wind anomalies (m/s) when tropical easterly waves are present in the regional model domain at 600 hPa in (a) ERA-5, (b) NCEP R2, (c) RR-RAS, and (d) RR-KF2 during May–November from 1986 to 2001.

in Figures 1c and 1d, respectively. This is similarly observed at 700 hPa (Figure S5 in Supporting Information S1) and 850 hPa (Figure S6 in Supporting Information S1). In all instances, the precipitation from TEWs in RR-KF2 exceeds RR-RAS and both model simulations underestimate the precipitation over northern Caribbean Sea relative to ERA5.

In further analyzing these contributions to total precipitation from TEWs, we also analyzed convective and stratiform precipitation. In Figure 8, we show the corresponding contribution of the convective (CP) and stratiform (SP) precipitation between the two models, which shows that contributions from both convective and stratiform precipitation in TEWs are higher in RR-KF2 than RR-RAS. This further explains the stronger response of in situ generation of TEWs in RR-KF2 compared with RR-RAS. Several earlier studies have indicated a coherent relationship between TEWs and convective activity, which leads to some of the regions being the preferred regions for TEWs (Carlson, 1969; Fink & Reiner, 2003; Kiladis et al., 2006; Mekonnen et al., 2006; Reed et al., 1977; Thorncroft et al., 2008; Torres et al., 2021). Additionally, Torres et al. (2021) show that the in situ generation of TEW is sensitive to the vertical profile of latent heating, with the stratiform type of precipitation generating the strongest response of TEWs in the IAS region. Our results appear to be consistent with these findings, with RR-KF2 showing a higher frequency of TEWs than RR-RAS. Similarly, Figures S7 and S8 in Supporting Information S1 show, as in Figure 8 in Supporting Information S1, the convective and stratiform precipitation contribution from TEWs in the regional models at 700 and 850 hPa, respectively. The results are like those in Figure 8, with RR-KF2 showing a higher contribution from both convective and stratiform type precipitation than RR-RAS.

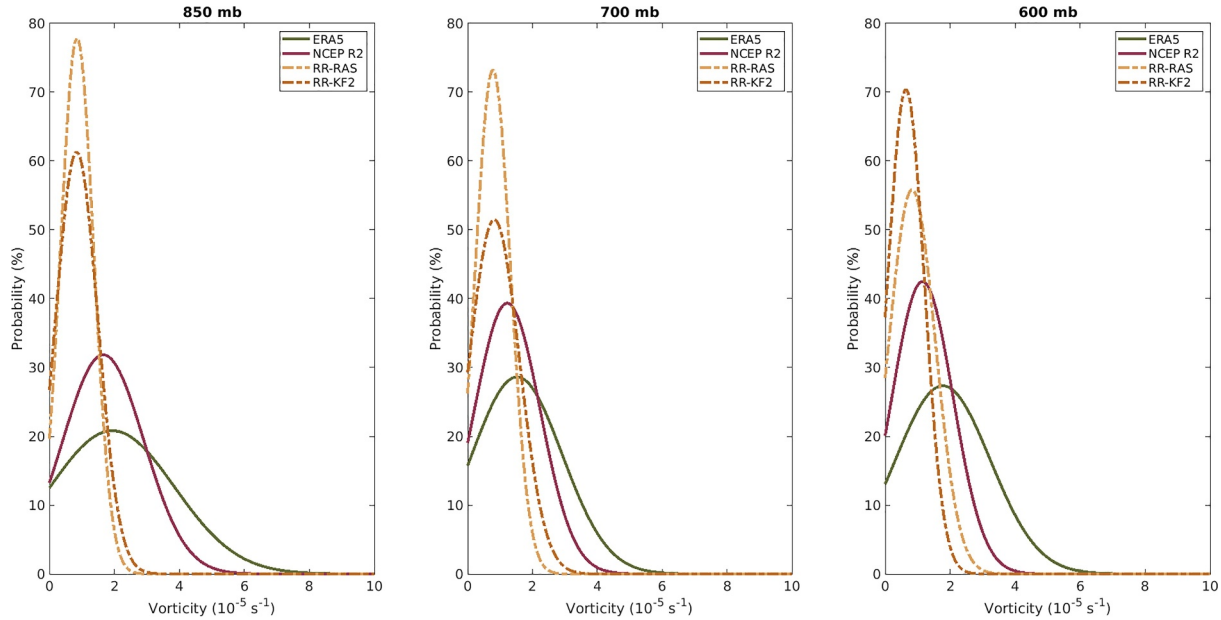

Figure 6. Probability density function of May–November average tropical easterly wave trough-axis relative vorticity at (a) 850 hPa, (b) 700 hPa, and (c) 600 hPa for 1986–2001. The ordinate represents the probability of the vorticity across the spectrum of vorticity in all the troughs of the Tropical Easterly Waves in the data set.

4.7. Tropical Cyclones

We have also plotted the track density of TS (which is the number of TS per 1° × 1° grid cell per 6 hr) from HURDAT2, ERA5, and the two regional models. In Figure 9a, HURDAT2 shows that TSs rarely occur south of 10°N both in the east Pacific and Caribbean Sea. Furthermore, the density is highest in the open east Pacific Ocean between latitudes of 10°N and 15°N and along the Caribbean coasts of Nicaragua, Honduras and Belize and further north along the Mexican coast of Gulf of Mexico (Figure 9a). Many of these features in HURDAT are replicated in ERA5 (Figure 9b), although the latter slightly underestimates both in the east Pacific and in the Caribbean Sea relative to the former. The RR-RAS simulation in Figure 9c shows a reasonable coverage of these TS in comparison to HURDAT2 in the east Pacific with majority of TS north of 10°N and the highest density of TS found in similar locations as HURDAT2. However, RR-RAS significantly underestimates TS in the Caribbean Sea compared with HURDAT2 or ERA5. On the other hand, RR-KF2 (Figure 9d) produces far more TS in the

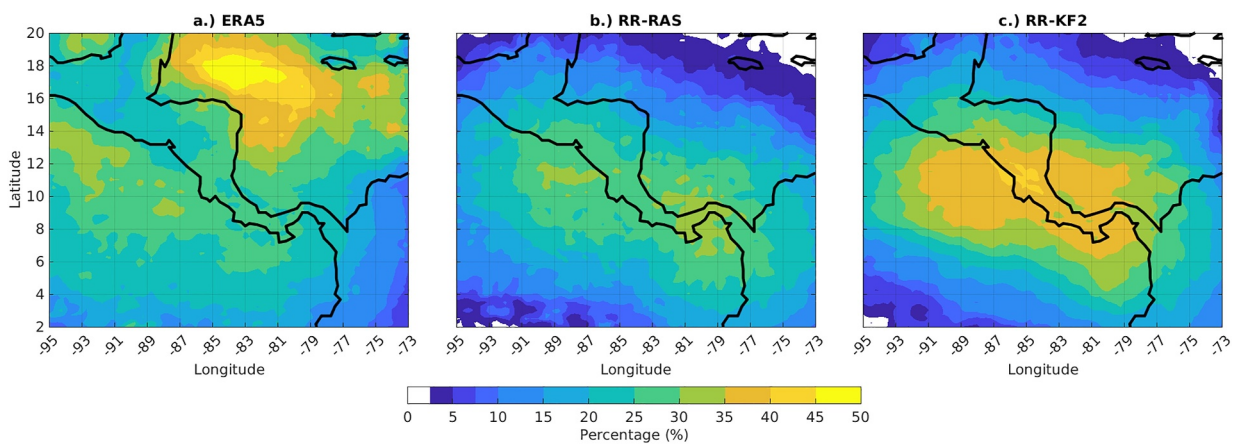

Figure 7. The percentage of May–November total precipitation attributed to tropical easterly waves present at 600 hPa from (a) ERA-5, (b) RR-RAS, and (c) RR-KF2. In (a) we use IMERGv7 data from 2001 to 2022 and in (b) and (c) we use the corresponding model output rain rates from 1986 to 2001.

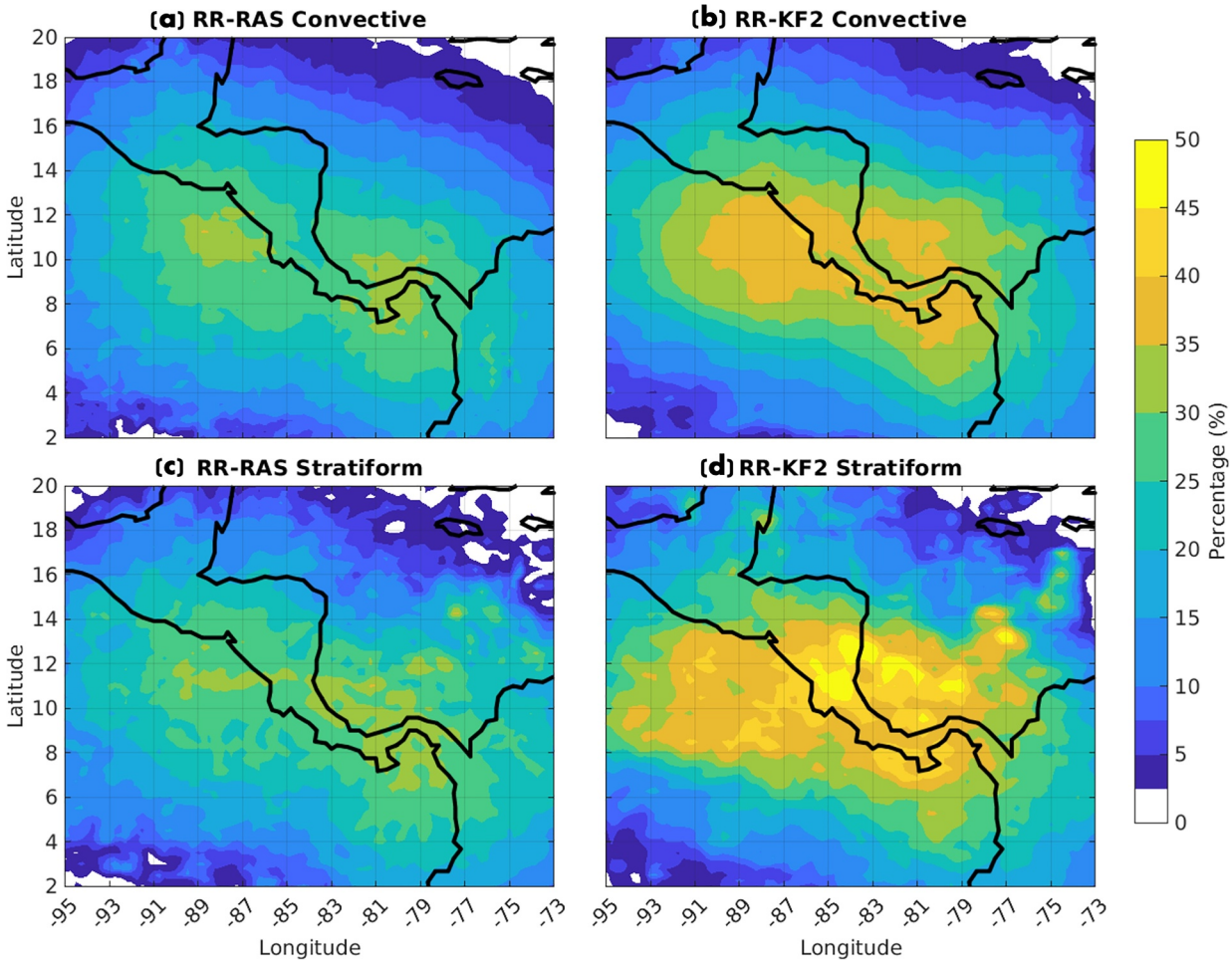

Figure 8. Percentage of May–November (a), (b) convective and (c), (d) stratiform precipitation attributed to tropical easterly waves present at 600 hPa in (a), (c) RR-RAS, and (b), (d) RR-KF2. RR-RAS and RR-KF2 use model output rain rates from 1986 to 2001.

east Pacific than HURDAT2 (Figure 9a), ERA5 (Figure 9b), and RR-RAS (Figure 9c). The TS simulation is slightly more comparable on the Caribbean Sea side between RR-KF2 and HURDAT2.

5. Discussion

The variations seen in the TEW features of the two regional climate simulations of RR-KF2 and RR-RAS in this study can be attributed to the differences in the cumulus parameterization schemes as that is the only difference between the simulations. Both the Relaxed Arakawa-Schubert (RAS) and Kain-Fritsch version 2 (KF2) schemes are well established parameterizations, developed over three decades ago. Notably, this study presents a unique comparison of these schemes in simulating TEWs within a coupled ocean-atmosphere framework, utilizing a higher resolution than most previous research conducted in the IAS region. It may be noted that only a small fraction (~15–25%) of TEWs generated both in the Caribbean Sea and in the tropical eastern Pacific eventually become TCs.

It is interesting to note that in terms of the amplitude and wavelength of the TEWs, both RR-RAS and RR-KF2 simulations are comparable. However, a major difference between the simulations is that RR-KF2 produces far more TEWs than RR-RAS (Figures 1 and 2), with both simulations displaying a bias of too many TEWs compared with ERA5. Furthermore, the excessive TEWs in the RR-KF2 simulation over the Panama Bight region, over Costa Rica, and off the coast of Guatemala and El Salvador suggest a strong influence of the coastal topography. For instance, in the vicinity of the northerly Panama Jet over the Panama Bight region and the easterly Papagayo Jet through northern Costa Rica and southern Nicaragua is where some of the densest TEWs

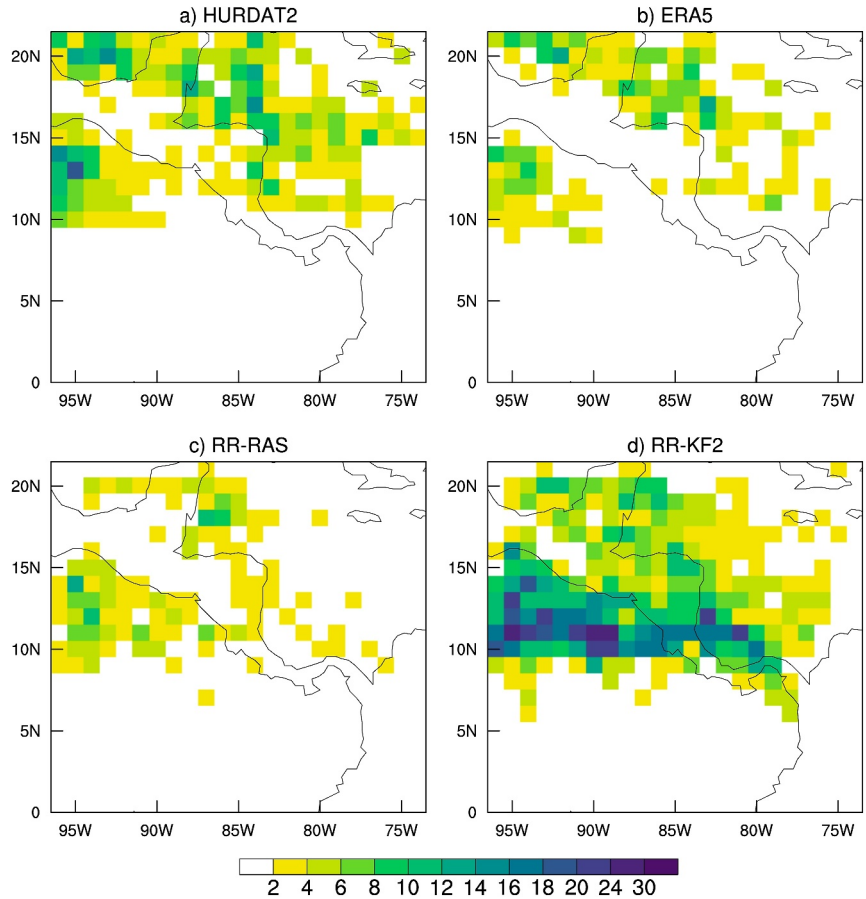

Figure 9. The track density plot of the Tropical Storms (TS; i.e., number of TS per 1° × 1° per 6 hr) from May to November from (a) HURDAT2, (b) ERA5, (c) RR-RAS, and (d) RR-KF2 simulation over the period of 1986–2001.

are observed in both simulations. Fuentes-Franco et al. (2015) noted from their modeling studies that TC genesis in the tropical northeastern Pacific is sensitive to these gap winds. Furthermore, we also find that both model simulations can produce TEWs in the IAS even when it is forced by a global reanalysis that produces hardly any TEWs in the domain. This latter point strongly suggests that the TEWs produced in RR-RAS and RR-KF2 are locally generated and are not as such (lateral) boundary forced.

The RAS scheme is based on *quasi-equilibrium theory*, where convection relaxes instability over a spectrum of cloud types. The gap winds serve as a significant source of low-level vorticity (Holbach & Bourassa, 2014; Whitaker & Maloney, 2020). In turn, low level vorticity is collocated with relatively strong convergence, moisture flux convergence, and upward motion (Chen & Gall, 1983) to which the RAS scheme responds with higher cloud base mass flux thus raising precipitation and modifying diabatic heating profiles with stronger upper tropospheric heating (Moorthi & Suarez, 1992). In fact, Zhang and McFarlane (1995) show that RAS type schemes perform better in regions of sustained low-level vorticity and moisture convergence, when quasi-equilibrium is more valid.

The KF2 scheme is *trigger-based* and uses parcel energetics to initiate convection. It is *more sensitive to transient convergence and vertical motion* than RAS (Kain, 2004). KF2 explicitly considers *low-level moisture convergence and vertical velocity* in its trigger mechanism. Vorticity maxima generated from the gap winds or TEWs enhance these terms, particularly on the eastern flank of the wave trough (e.g., Hopsch et al., 2010), making convective triggering more likely. Furthermore, stronger low-level vorticity increases boundary-layer moisture and reduces convective inhibition, which enables KF2 to select *more buoyant parcels*, enabling deeper convection. In addition, in regions of organized vorticity, KF2 can trigger *more vertically coherent plumes*, modifying vertical momentum and moisture transport, influencing wave propagation and downstream development (Hopsch et al., 2010; Kain, 2004; Raymond & Sessions, 2007).

Low-level vorticity acts as a *catalyst for convection* by modifying moisture convergence, vertical motion, and instability. Both RAS and KF2 respond to these environmental changes—RAS by increasing cloud ensemble activity to maintain equilibrium and KF2 by increasing triggering frequency and convective depth. However, KF2 tends to be *more responsive* to transient vorticity-induced convergence while RAS tends to *smooth the convective response* over time and space (Bechtold et al., 2001; Del Genio & Wu, 2010; Hohenegger & Bretherton, 2011; Yang et al., 2013). In our simulations RR-KF2 produces far higher amounts of convective precipitation in May–November period than RR-RAS (not shown), which can tilt and stretch pre-existing low-level vorticity to generate more TEWs in the former compared with the latter. Therefore, our results of RR-KF2 producing more TEWs and associated convective activity than RR-RAS are consistent with many of these previous studies.

RR-RAS and RR-KF2 simulations of this study is forced by a relatively older generation of atmospheric reanalysis of NCEP R2, which clearly has a bias of underrepresentation of TEWs. Nonetheless, both regional model simulations of this study can generate TEWs despite their weak forcing in the lateral boundaries of NCEP R2, suggesting an in situ generation of these waves, which is consistent with earlier studies (e.g., Rydbeck et al., 2017). The differences in the TEW simulations between RR-RAS and RR-KF2 occurs despite similar simulations of the LLJs in both model simulations (Figure S3 in Supporting Information S1), which is indicated to be one of the main sources of low level vorticity in the region (Holbach & Bourassa, 2014; Molinari et al., 1997; Molinari & Vollaro, 2000; Zehnder, 1991). We contend that it is the differing convective response of KF2 and RAS and the comparable large-scale conditions in the two model simulations that provides an insight to the differences in the TEWs between RR-RAS and RR-KF2 simulations.

6. Conclusions

In this study, we have dynamically downscaled a global reanalysis (NCEP R2) over the IAS region centered over Central America and analyzed for its simulation of the TEWs. These TEWs were analyzed at three pressure levels: 600, 700, and 850 hPa. Interestingly, the NCEP R2 has an extremely low occurrence of TEWs in the domain using the TEW detection algorithm following Belanger et al. (2017) across all three pressure levels. The two versions of the coupled ocean-atmosphere regional model with different cumulus parameterization schemes (RR-RAS and RR-KF2) produce far more TEWs than NCEP R2, which clearly suggests the in situ generation of these waves. The TEW features in the regional models were compared with ERA5 global reanalysis. This comparison revealed that the regional models produce far more TEWs than ERA5. In addition, the densest frequency of TEW appeared near the Papagayo and Panama LLJ exit regions. The comparison also indicates that the regional models tend to generate these TEWs with relatively shorter wavelength and amplitude and weaker trough-average vorticity than ERA5. The comparison between the regional models suggests that RR-KF2 produces far more TEWs in the domain with slightly longer wavelengths and large amplitudes than RR-RAS. These differences are largely attributed to the differences in the precipitation characteristics of the two cumulus parameterization schemes, with RR-KF2 generating a higher seasonal percentage of convective and stratiform precipitation attributed to TEWs than RR-RAS, which earlier studies have indicated produce a stronger response in TEWs.

Since this study was conducted with a regional coupled ocean-atmosphere model, the SST bias also plays a role. RR-RAS displays a stronger cold bias along the Pacific and Atlantic coasts of Central America, which is greatly diminished in RR-KF2. This bias also plays a key role in sustaining convection over these coastal regions, which eventually helps in the growth of the TEWs (e.g., Rydbeck et al., 2017). This study shows that dynamic downscaling has a benefit for the simulation of TEWs in the IAS region and can generate these waves even when the large-scale forcing to the model shows extremely erroneous statistics of these waves. However, it is difficult to suggest that one of the convection schemes is superior to the other because both exhibit their limitations and advantages. For instance, the TEW features of its amplitude and wavelength in RR-KF2 are slightly more reasonable in relation to ERA5. But the excessive TEWs and the consequent increased TS activity in RR-KF2 is undesirable relative to RR-RAS. Nonetheless, the study shows that TEWs are extremely sensitive to cumulus parameterization scheme, which raises the hope that the TEW simulations in these models could be improved by working further on these cumulus parameterization schemes. However, the contributions of the bias in the lateral boundary forcing to the regional model simulations of this study remains an unknown factor that will be explored in a future study.

Data Availability Statement

The IMERG rainfall from NASA was obtained from IMERG (2024). The ERA5 reanalysis data was from ERA5 (2024), the observed Best Track Data was from HURDAT2 (2024). The SODA v2.2.4 ocean reanalysis data was obtained from SODA (2022). The NCEP-DOE (R2) reanalysis data at 6 hourly interval was obtained from UCAR (2022). The tracks of the LPS are identified using the TempestExtremes Tracking Algorithm (2024). The tropical easterly wave tracking algorithm follows Belanger et al. (2017) and is available from TEW Tracking Algorithm (2024). The data and the code used to generate the figures in this paper are publicly available from DeLaune et al. (2025).

Acknowledgments
We acknowledge the support from NASA Grant 80NSSC22K0595. The IMERG data set was provided by the NASA/Goddard Space Flight Center and PPS which developed and computed the IMERG as a contribution to GPM and archived at the NASA GES DISC.

References

Agudelo, P. A., Hoyos, C. D., Curry, J. A., & Webster, P. J. (2011). Probabilistic discrimination between large-scale environments of intensifying and decaying African easterly waves. *Climate Dynamics*, *36*(7–8), 1379–1401. https://doi.org/10.1007/s00382-010-0851-x

Alpert, J., Kanamitsu, M., Caplan, P., Sela, J., & White, G. (1988). Mountain induced gravity wave drag parameterization in the NMC medium-range forecast model. In *Conference on numerical weather prediction, 8th, Baltimore, MD* (pp. 726–733).

Amador, J. A. (1998). A climatic feature of the tropical Americas: The trade wind easterly jet. *Top. Meteor. Oceanogr.*, *5*, 91–102.

Amador, J. A. (2008). The intra-Americas sea low-level jet: Overview and future research. *Annals of the New York Academy of Sciences*, *1146*(1), 153–188. https://doi.org/10.1196/annals.1446.012

Avila, L. A., & Pasch, R. J. (1992). Atlantic tropical systems of 1991. *Monthly Weather Review*, *120*(11), 2688–2696. https://doi.org/10.1175/1520-0493(1992)120<2688:atso>2.0.co;2

Avila, L. A., Pasch, R. J., & Jing, J. G. (2000). Atlantic tropical systems of 1996 and 1997: Years of contrasts. *Monthly Weather Review*, *128*(10), 3695–3706. https://doi.org/10.1175/1520-0493(2000)128<3695:atsoay>2.0.co;2

Bechtold, P., Chaboureau, J.-P., Beljaars, A., Betts, A. K., Köhler, M., Miller, M., et al. (2001). The simulation of the diurnal cycle of convection over land in a global model. *Quarterly Journal of the Royal Meteorological Society*, *127*, 865–888.

Belanger, J. I., Jelinek, M. T., & Curry, J. A. (2017). A climatology of easterly waves in the tropical Western hemisphere. *Geoscience Data Journal*, *3*(2), 40–49. https://doi.org/10.1002/gdj3.40

Burpee, R. W. (1972). The origin and structure of easterly waves in the lower troposphere of North Africa. *Journal of the Atmospheric Sciences*, *29*(1), 77–90. https://doi.org/10.1175/1520-0469(1972)029<0077:TOASOE>2.0.CO;2

Burpee, R. W. (1974). Characteristics of North African easterly waves during the summers of 1968 and 1969. *Journal of the Atmospheric Sciences*, *31*(6), 1556–1570. https://doi.org/10.1175/1520-0469(1974)031<1556:CONAEW>2.0.CO;2

Carlson, T. N. (1969). Synoptic histories of three African disturbances that developed into Atlantic hurricanes. *Monthly Weather Review*, *97*(3), 256–275. https://doi.org/10.1175/1520-0493(1969)097<0256:shotad>2.3.co;2

Carton, J. A., & Giese, B. S. (2008). A reanalysis of ocean climate using simple ocean data assimilation (SODA). *Monthly Weather Review*, *136*(8), 2999–3017. https://doi.org/10.1175/2007MWR1978.1

Chen, S. S., & Gall, R. L. (1983). An observational study of the structure and propagational characteristics of tropical easterly waves. *Journal of the Atmospheric Sciences*, *40*(1), 128–144.

Chou, M. D., & Lee, K. T. (1996). Parameterizations for the absorption of solar radiation by water vapor and ozone. *Journal of the Atmospheric Sciences*, *53*, 1203–1208. https://doi.org/10.1175/1520-0469(1996)0532.0.co;2

Chou, M. D., & Suarez, M. J. (1994). An efficient thermal infrared radiation parameterization for use in general circulation models. *NASA Technical Memorandum NASA-TM-104606*, *3*, 98. Retrieved from https://ntrs.nasa.gov/archive/nasa/casi.ntrs.nasa.%20gov/19950009331.pdf

Cook, K. H., & Vizy, E. K. (2010). Hydrodynamics of the Caribbean low-level jet and its relationship to precipitation. *Journal of Climate*, *23*(6), 1477–1494. https://doi.org/10.1175/2009JCLI3210.1

DeLaune, C. M., Misra, V., & Jayasankar, C. B. (2025). Dataset for Impact of dynamic downscaling on the simulation of Tropical Easterly Waves in the Intra-Americas Seas. [Dataset]. Retrieved from https://osf.io/zubme/

Del Genio, A. D., & Wu, J. (2010). The role of entrainment in the diurnal cycle of Continental convection. *Journal of Climate*, *23*(10), 2722–2738. https://doi.org/10.1175/2009jcli3340.1

Diaz, M., & Aiyyer, A. (2015). Absolute and convective instability of the African easterly jet. *Journal of the Atmospheric Sciences*, *72*(5), 1805–1826. https://doi.org/10.1175/JAS-D-14-0128.1

Diro, G. T., Giorgi, F., Fuentes-Franco, R., Walsh, K. J. E., Giuliani, G., & Coppola, E. (2014). Tropical cyclones in a regional climate change projection with RegCM4 over the CORDEX Central America domain. *Climate Change*, *125*(1), 79–94. https://doi.org/10.1007/s10584-014-1155-7

Dominguez, C., Done, J. M., & Bruyère, C. L. (2020). Easterly wave contributions to seasonal rainfall over the tropical Americas in observations and a regional climate model. *Climate Dynamics*, *54*(1), 191–209. https://doi.org/10.1007/s00382-019-04996-7

Druyan, L. M., & Fulakeza, M. (2011). The sensitivity of African easterly waves to eastern tropical Atlantic sea-surface temperatures. *Meteorology and Atmospheric Physics*, *113*(1–2), 39–53. https://doi.org/10.1007/s00703-011-0145-9

Ek, M. B., Mitchell, K. E., Lin, Y., Rogers, E., Grunmann, P., Koren, V., et al. (2003). Implementation of Noah land surface model advances in the national centers for environmental prediction operational mesoscale Eta model. *Journal of Geophysical Research*, *108*(D22), 8851. https://doi.org/10.1029/2002JD003296

ERA5. (2024). ERA5. Retrieved from https://www.ecmwf.int/en/forecasts/datasets/reanalysis-datasets/era5. Accessed on 1 November 2024.

Ezer, T., Arango, H., & Shchepetkin, A. F. (2002). Developments in terrain-following ocean models: Intercomparisons of numerical aspects. *Ocean Modelling*, *4*(3–4), 249–267. https://doi.org/10.1016/s1463-5003(02)00003-3

Ferreira, R. N., & Schubert, H. (1997). Barotropic aspects of ITCZ breakdown. *Journal of the Atmospheric Sciences*, *54*(2), 261–285. https://doi.org/10.1175/1520-0469(1997)054<0261:BAOIB>2.0.CO;2

Fink, A. H., & Reiner, A. (2003). Spatio-temporal variability of the relation between African easterly waves and West African Squall Lines in 1998 and 1999. *Journal of Geophysical Research*, *108*(D11), 4332. https://doi.org/10.1029/2002JD002816

Fuentes-Franco, R., Coppola, E., Giorgi, F., Pavia, E. G., Diro, G. T., & Graef, F. (2015). Inter-annual variability of precipitation over Southern Mexico and central America and its relationship to sea surface temperature from a set of future projections from CMIP5 GCMs and RegCM4 CORDEX simulations. *Climate Dynamics*, *45*(1–2), 425–440. https://doi.org/10.1007/s00382-014-2258-6

Gray, W. M. (1968). Global view of the origins of tropical disturbances and storms. *Monthly Weather Review*, *96*(10), 669–700. https://doi.org/10.1175/1520-0493(1968)096<0669:gvotoo>2.0.co;2

Haidvogel, D. B., Arango, H. G., Hedstrom, K., Beckmann, A., Malanotte-Rizzoli, P., & Shchepetkin, A. F. (2000). Model evaluation experiments in the North Atlantic Basin: Simulations in nonlinear terrain-following coordinates. *Dynamics of Atmospheres and Oceans*, *32*(3), 239–281. https://doi.org/10.1016/s0377-0265(00)00049-x

Ham, S., & Hong, S. Y. (2013). Sensitivity of simulated intraseasonal oscillation to four convective parameterization schemes in a coupled climate model. *Asia-Pacific Journal of Atmospheric Sciences*, *49*(4), 483–496. https://doi.org/10.1007/s13143-013-0043-9

Ham, S., Yoshimura, K., & Li, H. (2016). Historical dynamical downscaling for East Asia with the atmosphere and ocean coupled regional model. *Journal of the Meteorological Society of Japan*, *94A*, 199–208. https://doi.org/10.2151/jmsj.2015-046

He, X., Kim, H., Kirstetter, P. E., Yoshimura, K., Chang, E. C., Ferguson, C. R., et al. (2015). The diurnal cycle of precipitation in regional spectral model simulations over West Africa: Sensitivities to resolution and cumulus schemes. *Weather and Forecasting*, *30*(2), 424–445. https://doi.org/10.1175/waf-d-14-00013.1

Hersbach, H., Bell, W., Berrisford, P., Horanyi, A., Sabater, J. M., Nicolas, J., et al. (2020). The ERA5 global reanalysis. *Quarterly Journal of the Royal Meteorological Society*, *146*(730), 1999–2049. https://doi.org/10.1002/qj.3803

Hohenegger, C., & Bretherton, C. S. (2011). Simulating deep convection with a shallow convection scheme. *Atmospheric Chemistry and Physics*, *11*(20), 10389–10406. https://doi.org/10.5194/acp-11-10389-2011

Holbach, H. M., & Bourassa, M. A. (2014). The effects of gap-wind-induced vorticity, the monsoon trough, and the ITCZ on east Pacific tropical cyclogenesis. *Monthly Weather Review*, *142*(3), 1312–1325. https://doi.org/10.1175/mwr-d-13-00218.1

Hollis, M. A., Stachnik, J. P., Lewis-Merritt, C., McCrary, R. R., & Martin, E. R. (2024). Precipitation characteristics of easterly waves across the global tropics. *Journal of Geophysical Research: Atmospheres*, *129*(7), e2023JD039957. https://doi.org/10.1029/2023jd039957

Hong, S. Y., & Pan, H. L. (1996). Nonlocal boundary layer vertical diffusion in a medium-range forecast model. *Monthly Weather Review*, *124*(10), 2322–2339. https://doi.org/10.1175/1520-0493(1996)124<2322:nblvdi>2.0.co;2

Hopsch, S. B., Thorncroft, C. D., & Molinari, J. (2010). Convectively coupled easterly waves in a mesoscale model: A precursor to tropical cyclogenesis. *Monthly Weather Review*, *138*, 3434–3456.

Hsieh, J. S., & Cook, K. H. (2007). A study of the energetics of African easterly waves using a regional climate model. *Journal of the Atmospheric Sciences*, *64*(2), 421–440. https://doi.org/10.1175/jas3851.1

Huffman, G. J., Stocker, E. F., Bolvin, D. T., Nelkin, E. J., & Tan, J. (2019). GPM IMERG final precipitation L3 half hourly 0.1 degree 3 0.1 degree V06 at GES DISC. *Goddard Earth sciences data and information services center (GES DISC)*. https://doi.org/10.5067/GPM/IMERG/3B-HH/06

HURDAT2. (2024). HURDAT2 datasets are available through the NHC data archive portal [Dataset]. *National Hurricane Center*. Retrieved from https://www.nhc.noaa.gov/data/

IMERG. (2024). IMERG. Retrieved from https://gpm.nasa.gov/data/directory

Juang, H. M., & Kanamitsu, M. (1994). The NMC nested regional spectral model. *Monthly Weather Review*, *122*, 3–26. https://doi.org/10.1175/1520-0493(1994)1222.0.co;2

Kain, J., & Fritsch, M. (1993). Convective parameterization for mesoscale models: The Kain-Fritsch scheme. *Meteorological Monographs*, *24*, 165–170. https://doi.org/10.1007/978-1-935704-13-3_16

Kain, J. S. (2004). The Kain–Fritsch convective parameterization: An update. *Journal of Applied Meteorology*, *43*(1), 170–181. https://doi.org/10.1175/1520-0450(2004)043<0170:tkcpau>2.0.co;2

Kanamitsu, M., Ebusuzaki, W., Woollen, J., Yang, S.-K., Hnilo, J., Fiorino, M., & Potter, G. L. (2002). NCEP-DOE AMIP-II reanalysis (R-2). *Bulletin of the American Meteorological Society*, *83*, 1631–1643. https://doi.org/10.1175/bams-83-11-1631(2002)0832.3.co;2

Kiladis, G. N., Thorncroft, C. D., & Hall, N. G. (2006). Three-dimensional structure and dynamics of African easterly waves. Part I: Observations. *Journal of the Atmospheric Sciences*, *63*(9), 2212–2230. https://doi.org/10.1175/jas3741.1

Landsea, C. (1993). A climatology of intense (or major) Atlantic hurricanes. *Monthly Weather Review*, *121*(6), 1703–1713. https://doi.org/10.1175/1520-0493(1993)121<1703:acoima>2.0.co;2

Landsea, C. W., & Franklin, J. L. (2013). Atlantic hurricane database uncertainty and presentation of a new database format. *Monthly Weather Review*, *141*(10), 3576–3592. https://doi.org/10.1175/mwr-d-12-00254.1

Large, W. G., McWilliams, J. C., & Doney, S. C. (1994). Oceanic vertical mixing: A review and a model with a nonlocal boundary layer parameterization. *Reviews of Geophysics*, *32*(4), 363–403. https://doi.org/10.1029/94rg01872

Li, H., Kanamitsu, M., & Hong, S. Y. (2012). California reanalysis downscaling at 10 km using an ocean-atmosphere coupled regional model system. *Journal of Geophysical Research*, *117*(D12), D12118. https://doi.org/10.1029/2011jd017372

Lin, Y.-L., Robertson, K. E., & Hill, C. M. (2005). Origin and propagation of a disturbance associated with an African easterly wave as a precursor of hurricane Alberto (2000). *Monthly Weather Review*, *133*(11), 3276–3298. https://doi.org/10.1175/MWR3035.1

McBride, J. L., & Zehr, R. (1981). Observational analysis of tropical cyclone formation. Part II: Comparison of non-developing versus developing systems. *Journal of the Atmospheric Sciences*, *38*(6), 1132–1151. https://doi.org/10.1175/1520-0469(1981)038<1132:oaotcf>2.0.co;2

Mekonnen, A., Thorncroft, C. D., & Aiyyer, A. R. (2006). Analysis of convection and its association with African easterly waves. *Journal of Climate*, *19*(20), 5405–5421. https://doi.org/10.1175/JCLI3920.1

Mellor, G. L., & Yamada, T. (1982). Development of a turbulence closure model for geophysical fluid problems. *Reviews of Geophysics*, *20*(4), 851–875. https://doi.org/10.1029/rg020i004p00851

Misra, V., Jayasankar, C. B., Mishra, A. K., Mitra, A., & Murugavel, P. (2022). Dynamic downscaling the South Asian Summer Monsoon from a global reanalysis using a regional coupled ocean-atmosphere model. *Journal of Geophysical Research: Atmospheres*, *127*(22), e2022JD037490. https://doi.org/10.1029/2022JD037490

Molinari, J., Knight, D., Dickinson, M., Vollaro, D., & Skubis, S. (1997). Potential vorticity, easterly waves, and eastern Pacific tropical cyclogenesis. *Monthly Weather Review*, *125*(10), 2699–2708. https://doi.org/10.1175/1520-0493(1997)125<2699:pvewae>2.0.co;2

Molinari, J., & Vollaro, D. (2000). Planetary- and synoptic-scale influences on eastern Pacific tropical cyclogenesis. *Monthly Weather Review*, *128*(9), 3296–3307. https://doi.org/10.1175/1520-0493(2000)128<3296:passio>2.0.co;2

Molinari, J., Vollaro, D., Skubis, S., & Dickinson, M. (2000). Origins and mechanisms of Eastern Pacific Tropical Cyclogenesis: A case Study. *Monthly Weather Review*, *128*(1), 125–139. https://doi.org/10.1175/1520-0493(2000)128<0125:oamoep>2.0.co;2

Moorthi, S., & Suarez, M. J. (1992). Relaxed Arakawa-Schubert. A parameterization of moist convection for general circulation models. *Monthly Weather Review*, *120*(6), 978–1002. https://doi.org/10.1175/1520-0493(1992)1202.0.co;2

Pasch, R. J., & Avila, L. A. (1994). Atlantic Tropical systems of 1992. *Monthly Weather Review*, *122*(3), 539–548. https://doi.org/10.1175/1520-0493(1994)122<0539:atso>2.0.co;2

Peishu, Z., Jianping, T., Shuyu, W., Lingyun, X., Jianwei, Y., Yunqian, Z., et al. (2017). Dynamical downscaling of regional climate over eastern China using RSM with multiple physics scheme ensembles. *Theoretical and Applied Climatology*, *129*(3–4), 1263–1277. https://doi.org/10.1007/s00704-016-1847-1

Raymond, D. J., & Sessions, S. L. (2007). Evolution of convection during tropical cyclogenesis. *Geophysical Research Letters*, *34*(6), L06811. https://doi.org/10.1029/2006gl028607

Reed, R. J., Norquist, D. C., & Recker, E. E. (1977). The structure and properties of African Wave Disturbances as observed during Phase III of GATE. *Monthly Weather Review*, *105*(3), 317–333. https://doi.org/10.1175/1520-0493(1977)105<0317:TSAPOA>2.0.CO;2

Reynolds, R. W., Smith, T. M., Liu, C., Chelton, D. B., Casey, K. S., & Schlax, M. G. (2007). Daily high-resolution-blended analyses for sea surface temperature. *Journal of Climate*, *20*(22), 5473–5496. https://doi.org/10.1175/2007jcli1824.1

Rydbeck, A. V., Maloney, E. D., & Alaka Jr, G. J. (2017). In situ initiation of east Pacific easterly waves in a regional model. *Journal of the Atmospheric Sciences*, *74*(2), 333–351. https://doi.org/10.1175/jas-d-16-0124.1

Seo, H., Jochum, M., Murtugudde, R., Miller, A. J., & Roads, J. O. (2008). Precipitation from African easterly waves in a coupled model of the tropical Atlantic. *Journal of Climate*, *21*(6), 1417–1431. https://doi.org/10.1175/2007jcli1906.1

Serra, Y. L., Kiladis, G. N., & Hodges, K. I. (2010). Tracking and mean structure of easterly waves over the intra-americas sea. *Journal of Climate*, *23*(18), 4823–4840. https://doi.org/10.1175/2010JCLI3223.1

Shchepetkin, A. F., & McWilliams, J. C. (2005). The regional oceanic modeling system (ROMS): A split-explicit, free-surface, topography-following-coordinate Oceanic model. *Ocean Modelling*, *9*(4), 347–404. https://doi.org/10.1016/j.ocemod.2004.08.002

SODA. (2022). SODA. Retrieved from https://apdrc.soest.hawaii.edu/erddap/griddap/hawaii_soest_c71f_e12b_37f8.html. Accessed on 4 October 2022.

TempestExtremes Tracking Algorithm. (2024). Tracking algorithm used to track tropical storms [Software]. *Tracking algorithm used to track tropical storms*. Retrieved from https://github.com/ClimateGlobalChange/tempestextremes

TEW Tracking Algorithm. (2024). Tracking algorithm used to track Tropical Easterly waves [Software]. *Tracking algorithm used to track Tropical Easterly waves*. Retrieved from ftp://ftp.ncdc.noaa.gov/pub/data/aewc-v1/src/src_readme.docx

Thorncroft, C. D., Hall, N. M. J., & Kiladis, G. N. (2008). Three-dimensional structure and dynamics of African easterly waves. Part III: Genesis. *Journal of the Atmospheric Sciences*, *65*(11), 3596–3607. https://doi.org/10.1175/2008JAS2575.1

Tiedtke, M. (1983). The sensitivity of the time-mean large-scale flow to cumulus convection in the ECMWF model. In *Proceedings of ECMWF workshop on convective in large-scale models* (pp. 297–316). European Centre for Medium-Range Weather Forecasts.

Toma, V. E., & Webster, P. J. (2010). Oscillations of the intertropical convergence zone and the genesis of easterly waves. Part I: Diagnostics and theory. *Climate Dynamics*, *34*(4), 587–604. https://doi.org/10.1007/s00382-009-0584-x

Torres, V. M., Thorncroft, C. D., & Hall, N. M. J. (2021). Genesis of easterly waves over the tropical Eastern Pacific and the intra-americas Sea. *Journal of the Atmospheric Sciences*, *78*(10), 3263–3279. https://doi.org/10.1175/JAS-D-20-0389.1

UCAR. (2022). UCAR. Retrieved from https://rda.ucar.edu/datasets/ds091.0/

Ullrich, P. A., & Zarzycki, C. M. (2017). TempestExtremes: A framework for scale-insensitive pointwise feature tracking on unstructured grids [Software]. *Geoscientific Model Development*, *10*(3), 1069–1090. https://doi.org/10.5194/gmd-10-1069-2017

Ullrich, P. A., Zarzycki, C. M., McClenny, E. E., Pinheiro, M. C., Stansfield, A. M., & Reed, K. A. (2021). TempestExtremes v2. 1: A community framework for feature detection, tracking, and analysis in large datasets. *Geoscientific Model Development*, *14*(8), 5023–5048. https://doi.org/10.5194/gmd-14-5023-2021

Umlauf, L., & Burchard, H. (2003). A generic length-scale equation for geophysical turbulence models. *Journal of Marine Research*, *61*(2), 235–265. https://doi.org/10.1357/002224003322005087

Wang, C. (2007). Variability of the Caribbean low-level jet and its relations to climate. *Climate Dynamics*, *29*(4), 411–422. https://doi.org/10.1007/s00382-007-0243-z

Wang, C., & Enfield, D. B. (2001). The tropical Western hemisphere warm pool. *Geophysical Research Letters*, *28*(8), 1635–1638. https://doi.org/10.1029/2000gl011763

Whitaker, J. W., & Maloney, E. D. (2020). Genesis of an east Pacific easterly wave from a Panama Bight MCS: A case study analysis from June 2012. *Journal of the Atmospheric Sciences*, *77*(10), 3567–3584. https://doi.org/10.1175/JAS-D-20-0032.1

Yang, G.-Y., Slingo, J., & Hoskins, B. J. (2013). Convectively coupled equatorial waves in the MetUM: The role of the convection scheme. *Quarterly Journal of the Royal Meteorological Society*, *139*, 586–600.

Zehnder, J. A. (1991). The interaction of planetary-scale tropical easterly waves with topography: A mechanism for the initiation of tropical cyclones. *Journal of the Atmospheric Sciences*, *48*(10), 1217–1230. https://doi.org/10.1175/1520-0469(1991)048<1217:tiopst>2.0.co;2

Zhang, G. J., & McFarlane, N. A. (1995). Sensitivity of climate simulations to the parameterization of cumulus convection in the Canadian climate centre general circulation model. *Atmosphere-Ocean*, *33*(3), 407–446. https://doi.org/10.1080/07055900.1995.9649539

Zhao, Q., & Carr, F. H. (1997). A prognostic cloud scheme for operational NWP models. *Monthly Weather Review*, *125*(8), 1931–1953. https://doi.org/10.1175/1520-0493(1997)125<1931:apcsfo>2.0.co;2

Supplementary Material

Impact of dynamic downscaling on the simulation of Tropical Easterly Waves in the Intra-Americas Seas

Connor DeLaune[1, 2], Vasubandhu Misra[1, 2, #] and C. B. Jayasankar[2]

[1]Department of Earth, Ocean and Atmospheric Science, Florida State University, Tallahassee, Florida, U.SA.

[2]Center for Ocean-Atmospheric Prediction Studies, Florida State University, Tallahassee, Florida, U.SA.

Corresponding Author Email: vmisra@fsu.edu

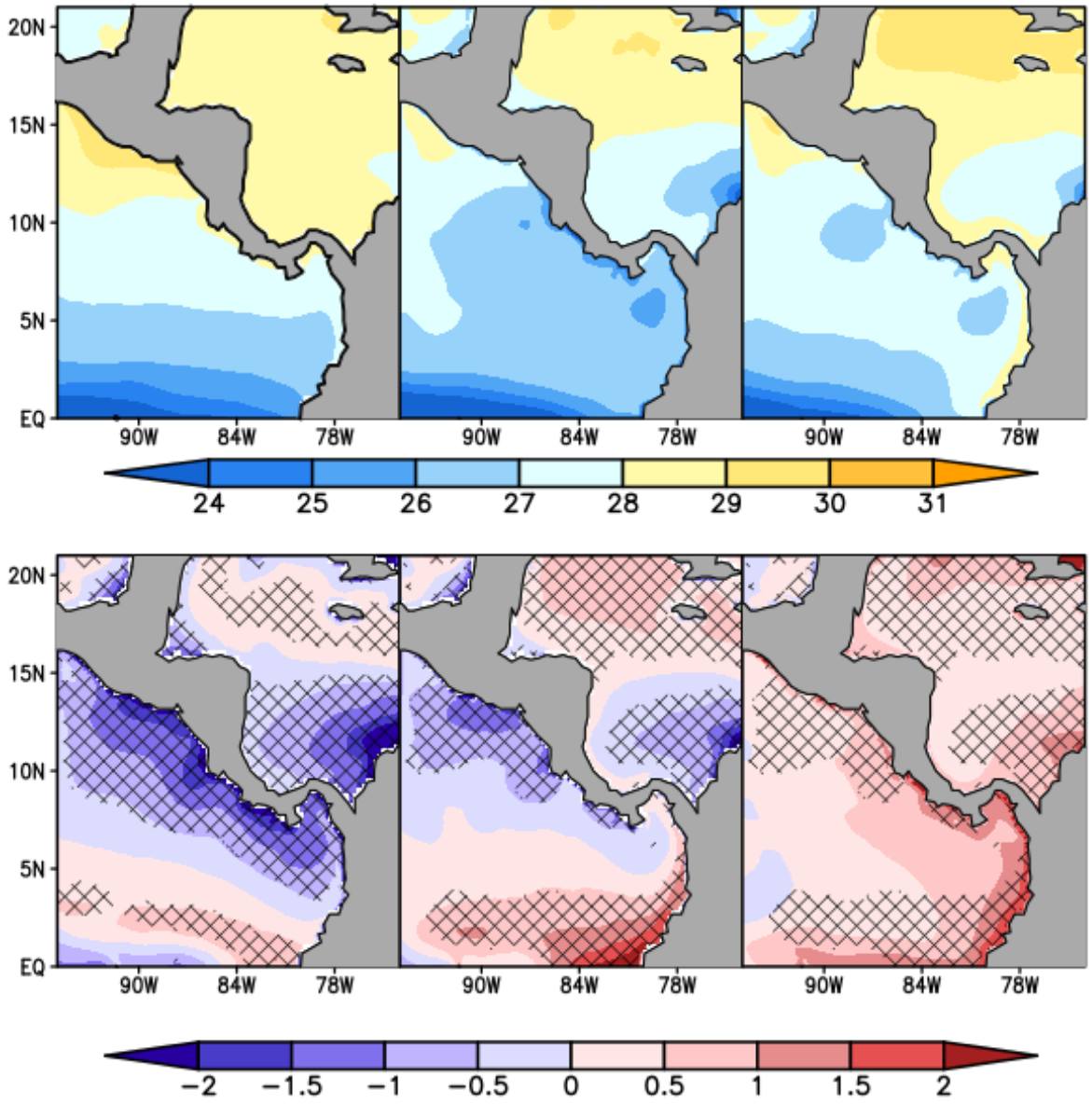

Figure S1: The May-November climatological mean SST (°C; shaded) from (a) observations, (b) RR-RAS, and (c) RR-KF2. The corresponding systematic errors of SST (°C) from (d) RR-RAS and (e) RR-KF2. (f) The difference between (RR-KF2)-(RR-RAS) in °C. The differences in (d), (e), and (f) are hatched only if they exceed 95% confidence interval according to t-test.

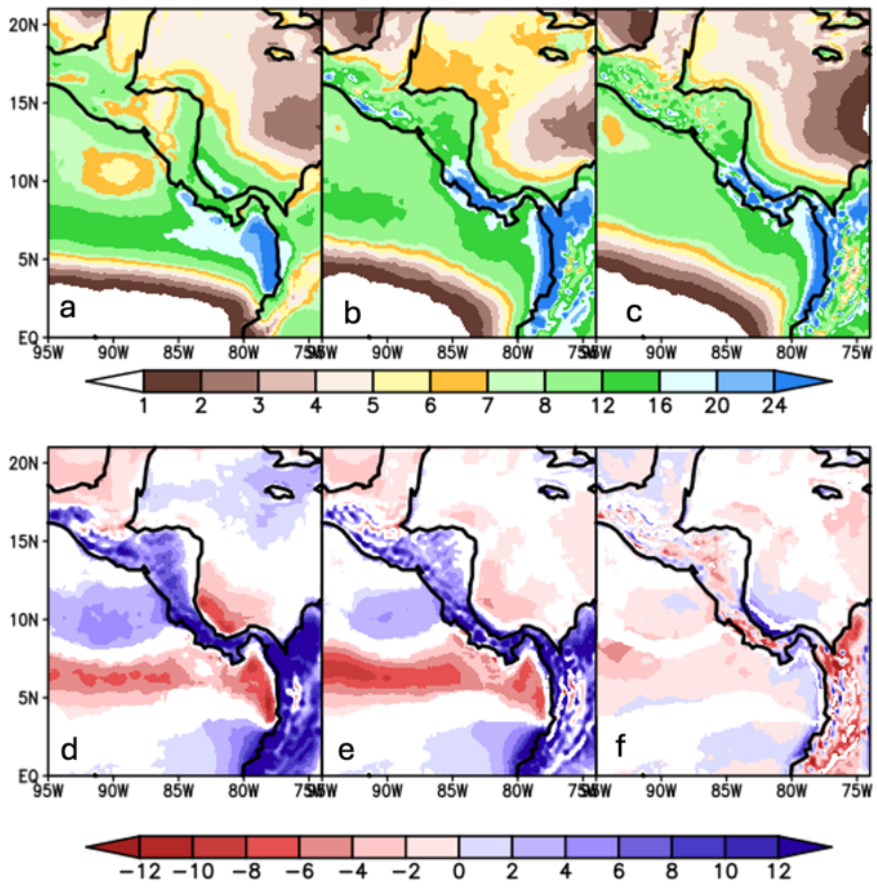

Figure S2: The May-November climatological mean precipitation (mm day^{-1}; shaded) from (a) observations, (b) RR-RAS, and (c) RR-KF2. The corresponding systematic errors of mean precipitation (mm day^{-1}) from (d) RR-RAS and (e) RR-KF2. (f) The difference between (RR-KF2)-(RR-RAS) in mm day^{-1}. The differences in (d), (e), and (f) are shaded only if they exceed 95% confidence interval according to t-test.

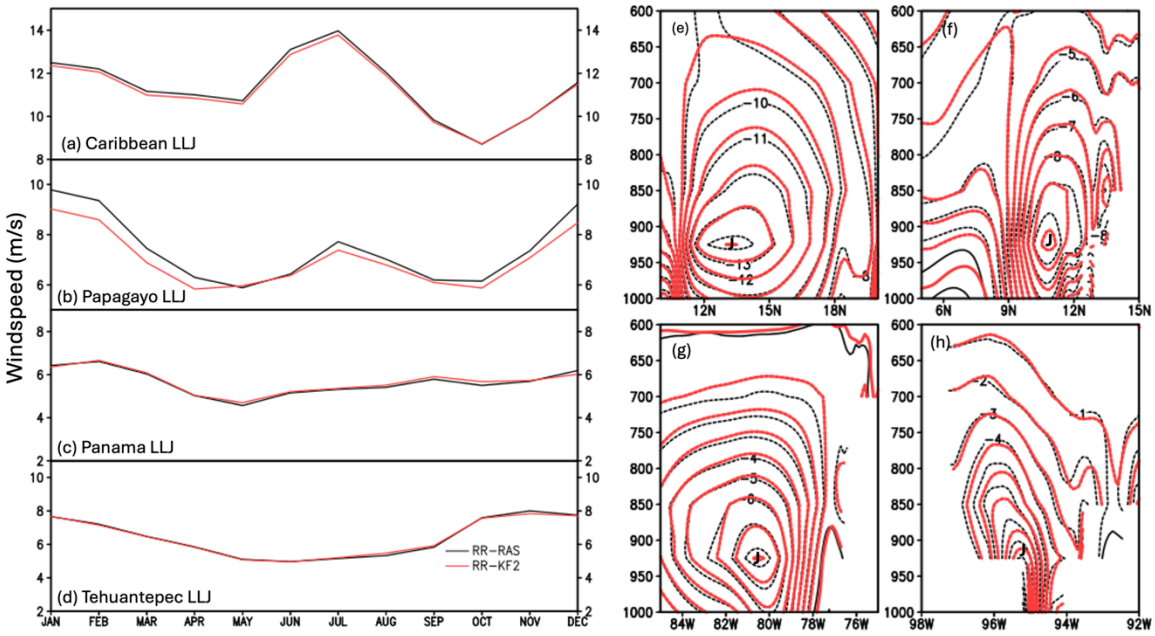

Figure S3: The climatological monthly mean timeseries of the wind speed indices of the a) Caribbean (78°W-78°W and 13°N-15°N), b) Papagayo (89°W-85°W and 9°N-11°N), c) Panama (80°W-78°W and 3°N-7°N), and d) Tehuantepec (96°W-94°W and 15°N-17°N) Low Level Jets (LLJs). These indices are computed at 925hPa. The corresponding monthly mean climatological vertical cross-section in the lower troposphere from 1000 to 600 hPa at their month of annual peak for the e) zonal wind of the Caribbean LLJ (CLLJ) at 75.5°W in July, f) zonal wind of the Papagayo LLJ at 87°W in January, g) meridional wind of the Panama LLJ at 5°N in February, and h) meridional wind of the Tehuantepec LLJ at 16°N in November. The dotted black and red contour lines in (e-h) correspond to RR-RAS and RR-KF2 respectively. The contour interval is 1 m/s in (e-h). The core of the jet is represented by J in (e-h).

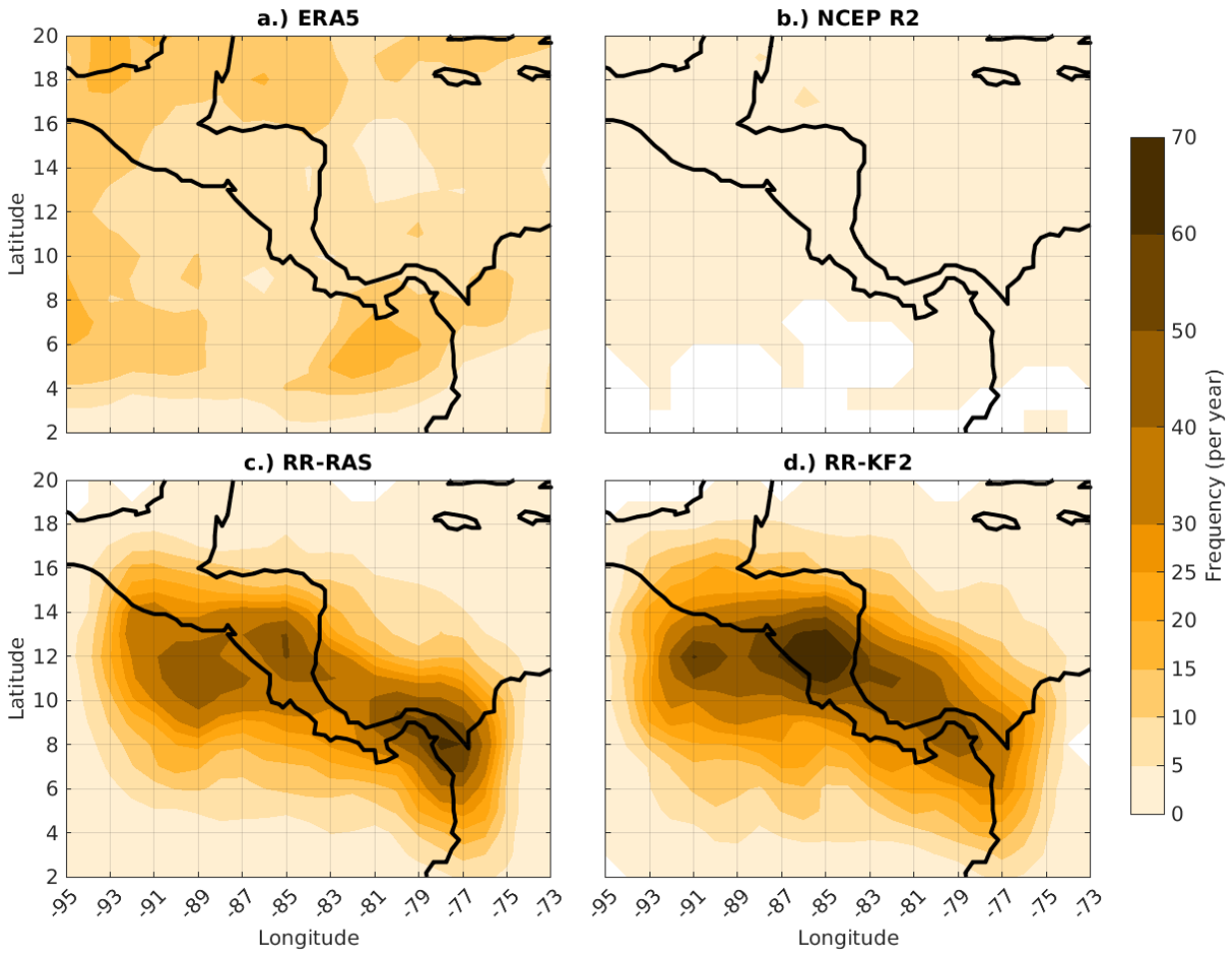

Figure S4: May-November average tropical easterly wave track density at 850 hPa for (a) ERA5, (b) NCEP R2, (c) RR-RAS, and (d) RR-KF2 for 1986-2001.

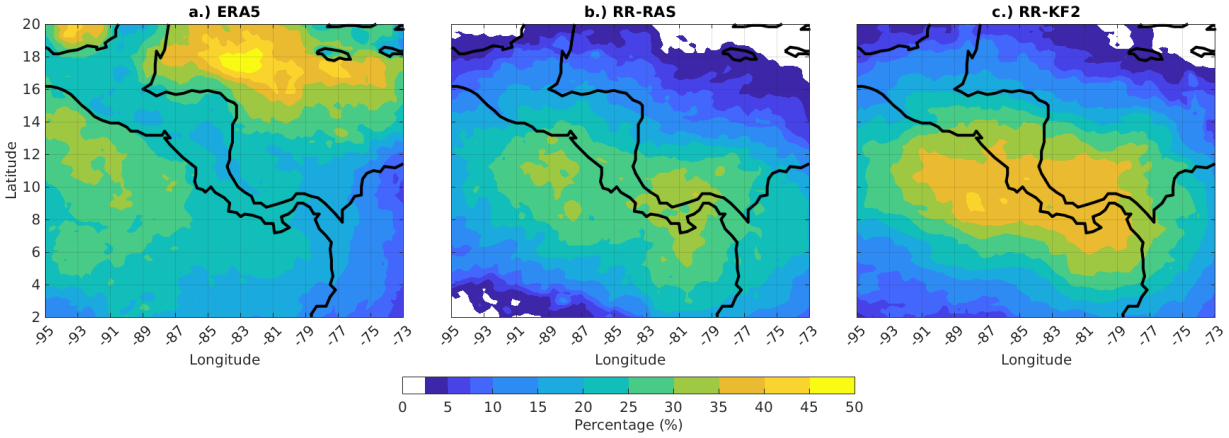

Figure S5: Percentage of May-November total precipitation attributed to tropical easterly waves present at 700hPa in a) ERA-5, b) RR-RAS, and c) RR-KF2. ERA5 uses IMERGv7 data from 2001-2022, and RR-RAS and RR-KF2 use model output rain rates from 1986-2001.

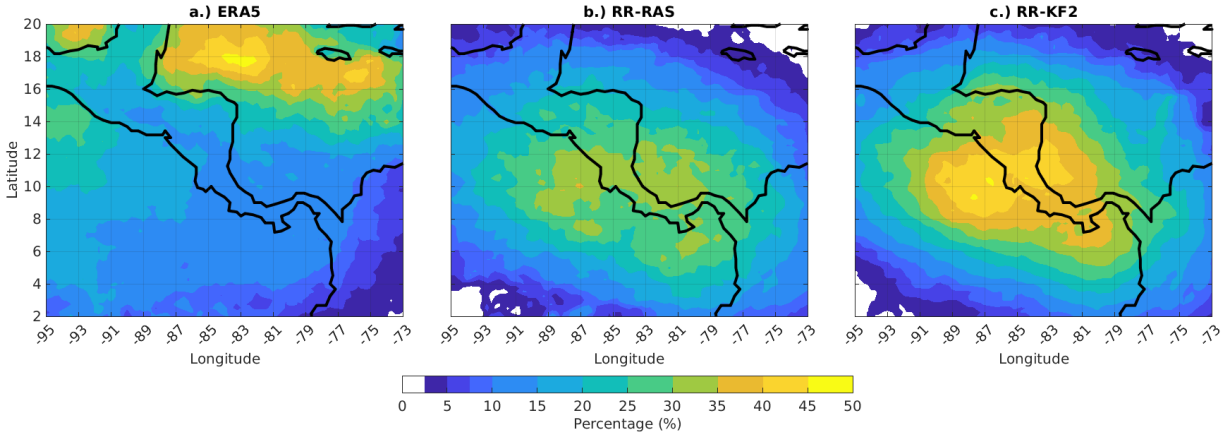

Figure S6: Percentage of May-November total precipitation attributed to tropical easterly waves present at 850hPa in a) ERA-5, b) RR-RAS, and c) RR-KF2. ERA5 uses IMERGv7 data from 2001-2022, and RR-RAS and RR-KF2 use model output rain rates from 1986-2001.

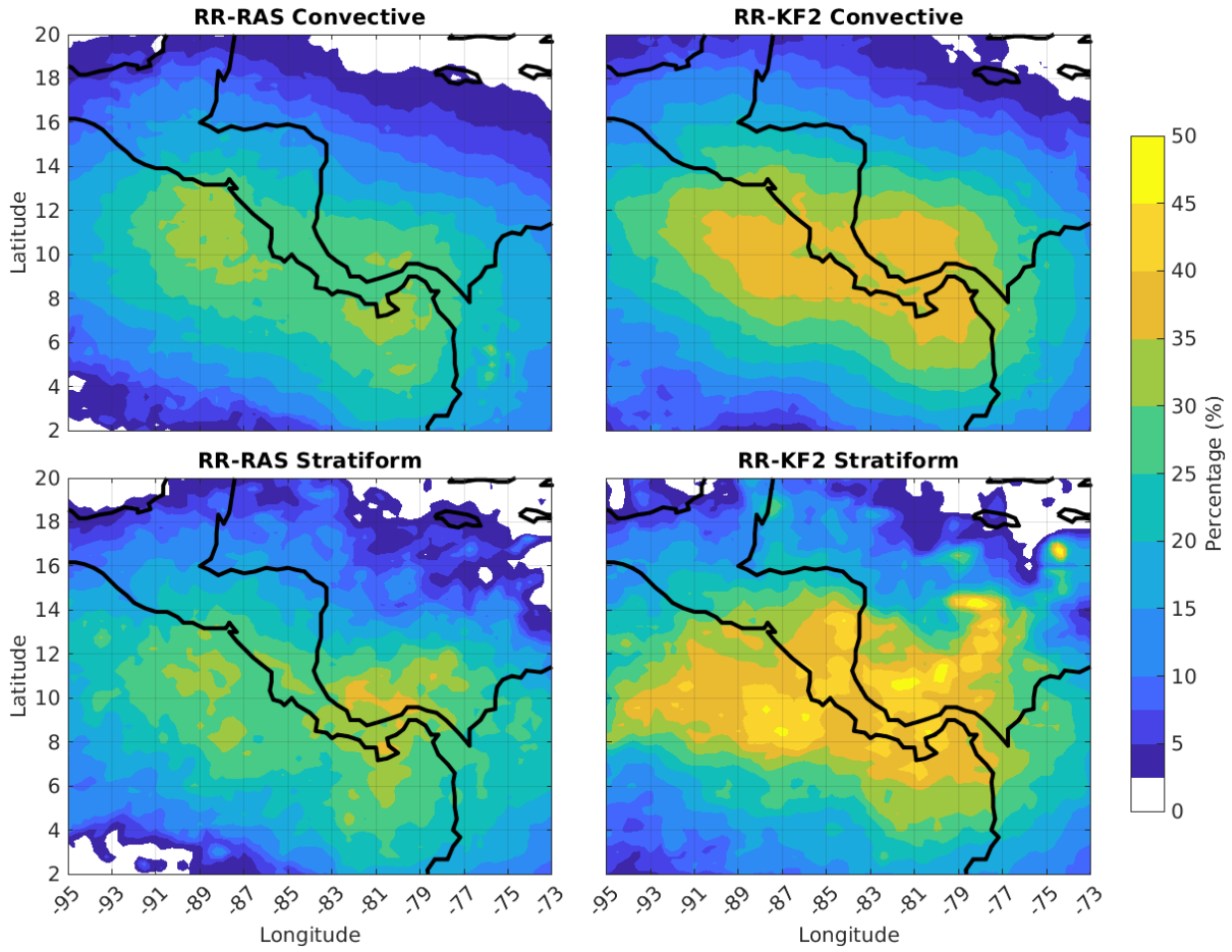

Figure S7: Percentage of May-November (a, b) convective and (c, d) stratiform precipitation attributed to tropical easterly waves present at 700 hPa in (a, c) RR-RAS, and (b, d) RR-KF2. RR-RAS and RR-KF2 use model output rain rates from 1986-2001.

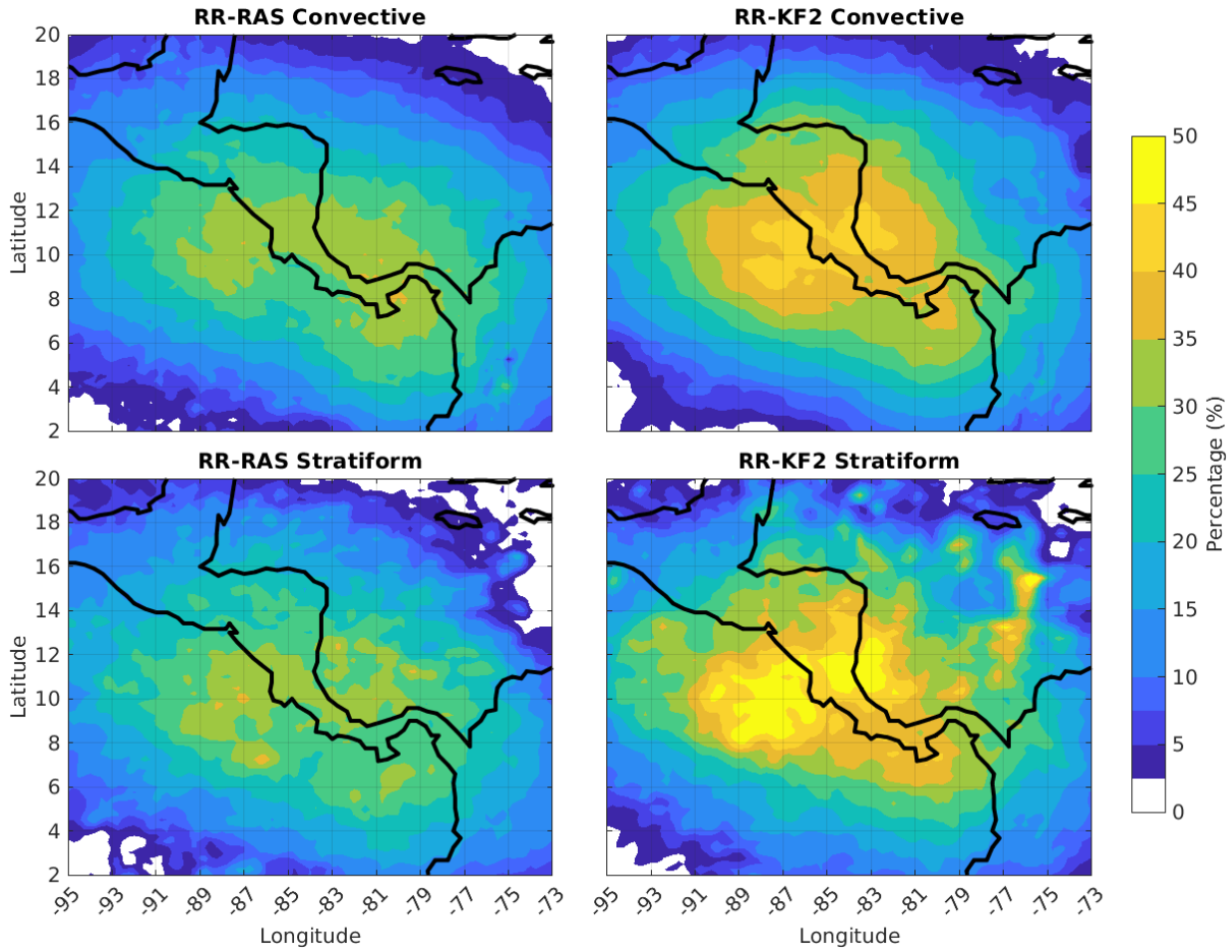

Figure S8: Percentage of May-November (a, b) convective and (c, d) stratiform precipitation attributed to tropical easterly waves present at 850 hPa in (a, c) RR-RAS, and (b, d) RR-KF2. RR-RAS and RR-KF2 use model output rain rates from 1986-2001.